



Multiphase-solid fluid inclusions in HP-LT eclogite facies rock (Zavkhan Terrane, Western Mongolia): evidence for the evolution from saline to hypersaline fluids during metamorphism in subduction zone

Manzshir Bayarbold^{1,2} · Atsushi Okamoto¹ · Masaoki Uno¹ · Kenta Yoshida³ · Alexey Kotov¹ · Geri Agroli¹ · Otgonbayar Dandar^{1,2} · Yasuhiro Niwa⁴ · Masao Kimura⁴ · Noriyoshi Tsuchiya¹

Received: 29 January 2023 / Accepted: 28 August 2023
© The Author(s) 2023

Abstract

Fluid inclusions in high- and ultrahigh-pressure metamorphic rocks provide direct information on the composition of the fluids that evolved during metamorphism and fluid-rock interactions in deep subduction zones. We investigate the fluid inclusions in the Khungui eclogite of the Zavkhan Terrane, Central Asian Orogenic Belt. Fluid inclusions are observed in garnet and quartz in the eclogite samples that underwent metamorphism during subduction. The primary fluid inclusions in quartz are composed of liquid and vapor with high salinities (15.7–16.4 wt.% NaCl eq.), whereas the secondary fluid inclusions in quartz are classified as: relatively high salinity (Type I: 12.5–16.3 wt.% NaCl eq.) and low salinity (Type II: 6.7–10.6 wt.% NaCl eq.). The garnet shows compositional zoning from Ca-poor cores to Ca-rich rims, and the rims that grew during the eclogite-stage metamorphism (2.1–2.2 GPa at 580–610 °C) preferentially contain numerous primary fluid inclusions. The primary fluid inclusions in garnet are commonly bi-phases (liquid and vapor); however, some are multiphase-solid fluid inclusions composed of fluids (liquid and vapor) and combinations of several minerals (halite, quartz, apatite, calcite, biotite, chlorite, and actinolite). Bi-phase fluid inclusions preferentially occur in the inner parts of the Ca-rich garnet rim, whereas multiphase-solid fluid inclusions occur along the margins of the Ca-rich rim. We hypothesize that the multiphase-solid fluid inclusions are formed via interactions between trapped fluids, trapped minerals, and the host garnet during exhumation. By combination of FIB–SEM and synchrotron X-ray CT analyses, the detailed occurrences, volumes, and compositions of the solid phases in the fluid inclusion was analyzed. We then conduct mass balance analysis to reconstruct accurate fluid compositions using data from the FIB–SEM and synchrotron X-ray CT images of the multiphase-solid fluid inclusion. The results of these analyses reveal that (1) fluid changed from an H₂O-dominated saline fluid (13–16 wt. % NaCl eq.) at the prograde to the earlier eclogite stage to H₂O–CO₂-dominated hypersaline fluid at later eclogite stage (~32 wt. % NaCl eq., 7.3 wt. % CO₂ and ~19 molal dissolved cations); (2) a variety of mineral assemblages in multiphase-solid fluid inclusions are produced by post-entrapment reactions between the trapped hypersaline fluid, trapped minerals and the fluid host mineral. The evolution of fluids from saline to hypersaline during the eclogite facies stage is probably caused by the formation of hydrous minerals (i.e., barroisite) under a near-closed system.

Keywords Multiphase-solid fluid inclusion · H₂O-dominated fluid · Hypersaline fluid · Eclogite · Zavkhan Terrane

Communicated by Daniela Rubatto.

✉ Noriyoshi Tsuchiya
noriyoshi.tsuchiya.e6@tohoku.ac.jp

¹ Graduate School of Environmental Studies, Tohoku University, Sendai, Japan

² Geoscience Center, Mongolian University of Science and Technology, Ulaanbaatar, Mongolia

³ Japan Agency for Marine-Earth Science and Technology (JAMSTEC), Research Institute for Marine Geodynamics, Yokosuka, Japan

⁴ Photon Factory, Institute of Materials Structure Science, High Energy Accelerator Research Organization (KEK), Tsukuba, Japan

Introduction

High-pressure (HP) and ultrahigh-pressure (UHP) metamorphic rocks are exhumed along suture zones in paleo-orogenic metamorphic terranes. Petrological analyses of such rocks provide critical information on the evolution of deep fluids and fluid–rock interactions within subduction zones (Giaramita and Sorensen 1994; Scambelluri et al. 1998; Xiao et al. 2000, 2002, 2006; Scambelluri and Philippot 2001; Fu et al. 2001, 2002, 2003b; Gao and Klemd 2001; Ferrando et al. 2005a; Zhang et al. 2005, 2006, 2008; Li et al. 2006; Frezzotti et al. 2007; Korsakov et al. 2011; Kawamoto et al. 2018; Liu et al. 2019).

In recent decades, numerous natural and experimental studies have revealed that deep fluids within subduction zones are made up of multiple compounds, primarily volatile compounds (C, O, H, N, S), and that they subordinate to high amounts of organic acids and hydrocarbons, non-volatile substances (Si, Al, Ca, Mg, Fe, K, Na, Cl), dissolved molecular materials (S–Cl–Si–C), and ligands (SO_4^{2-} , HCO_3^- , CO_3^{2-} , HSiO_3^- , Cl^-) (Philippot and Selverstone 1991; Philippot et al. 1995; Frezzotti et al. 2011; Okamoto et al. 2014; Frezzotti and Ferrando 2015). This has also been predicted using thermodynamic models (Galvez et al. 2016; Connolly and Galvez 2018; Huang and Sverjensky 2019; Maffei et al. 2021; Okamoto et al. 2021).

The presence of multiphase-solid fluid inclusions in the HP and UHP rocks confirms that multi compounds are present in deep fluids within subduction zones. Such fluid inclusions with variable salinities (~ 13–60 wt.% NaCl eq.) have been reported in UHP metamorphic rocks in metamorphic belts such as the Dabie–Sulu orogenic belt in China (Shen et al. 2003; Ferrando et al. 2005b, a; Zhang et al. 2005, 2008), the Tauern Window, and the Dora–Maira massif in the European Alps (Selverstone et al. 1992; Maffei et al. 2021), and the Western Gneiss Region in Norway (Svensen et al. 1999; Svensen and Museum 2001). Mineralogical and petrological studies of multiphase-solid inclusions in UHP metamorphic rocks have revealed that most minerals present in the fluids contain a diverse range of major elements (Si, Al, Mg, Fe, Ca, Na, and K) and trace elements (Ti, Zr, Ba, and high field strength elements), that form silicate minerals such as mica, amphibole, and epidote (Frezzotti and Ferrando 2015). Such inclusions rarely contain silica minerals, diamonds, phosphates, carbonates, sulfates, or chlorides (Stöckhert et al. 2001; van Roermund et al. 2002).

Several studies have tried to reconstruct the compositions of the trapped fluids observed as multiphase-solid fluid inclusions in HP and UHP rocks found in various regions, for example, the Dabie–Sulu orogenic belt in

China (Xiao et al. 2000; Fu et al. 2001; Ferrando et al. 2005a, b; Zhang et al. 2005; Frezzotti et al. 2007; Jin et al. 2023), the Dora–Maira massif in Italy (Philippot et al. 1995; Ferrando et al. 2009, 2017; Maffei et al. 2021), the Kokchetav massif in northern Kazakhstan (De Corte et al. 1998; Hwang et al. 2003; Dobrzhinetskaya et al. 2005; Korsakov et al. 2011; Mikhno et al. 2014; Stepanov et al. 2014, 2016) and the Erzgebirge massif in Germany (Hwang et al. 2001, 2006; Stöckhert et al. 2001, 2009; Dobrzhinetskaya et al. 2003b). However, quantitative reconstruction of fluid compositions from the multiphase fluid inclusions is not always easy due to two possible reasons. First, the formation of solid phases in fluid inclusions may not be due to precipitation from aqueous fluids or crystallization from hydrous silica melts (Ferrando et al. 2005a), but may have formed during reactions with host minerals after fluid trapping (Philippot and Selverstone 1991; Selverstone et al. 1992; Scambelluri et al. 1998; Svensen and Museum 2001; Perchuk et al. 2005, 2008; Korsakov et al. 2011; Korsakov 2018). Therefore, detailed studies on the microstructural relationships of these rocks are required to determine how these minerals were formed and whether any reactions occurred within the inclusions. Second, previous attempts to quantitatively reconstruct fluid compositions were mostly based on 2D-observations using optical microscopes, which generated significant errors in the volume estimates of the individual phases used for mass balance analyses (Ferrando et al. 2005a; Frezzotti et al. 2007). Recently, 3D-phase analyses of the multiphase fluid- and void-bearing inclusions has become possible using micro-Raman imaging, which can even be used on high-grade metamorphic rocks (e.g., Dabie–Sulu; Jin et al. 2023); however, the spatial resolution of Raman imaging is limited to several hundred nanometers, which makes it difficult to analyze small (< 10 μm) inclusions that are common in metamorphic rocks.

In this paper, we report the results of our investigation of fluid inclusions in the Khungui eclogite, found in the northern part of the Central Asian Orogenic Belt (CAOB). Numerous primary and secondary fluid inclusions are present in the garnet and quartz of this eclogite. Moreover, various types of multiphase-solid fluid inclusions occur in compositionally zoned garnets, the rims of which correspond to the eclogite stage of metamorphism. Based on the textures, mineralogy, and microthermometry of fluid inclusions, we determine the variations in salinity and fluid composition in the Khungui eclogite at various stages of its metamorphic history. Furthermore, this is the first report of using 3D-X-ray CT images of multiphase-solid fluid inclusion in garnet to reconstruct the fluid compositions during the eclogite stage of metamorphism. We use these new findings to speculate on the possible mechanisms underlying the mineralogical variation in these multiphase-solid fluid inclusions.

Geological setting

The CAOB is a giant Paleozoic orogenic belt that extends east–west from the Caspian Sea to the northern west Pacific Ocean (Fig. 1a). Most researchers argue that four main subduction systems were involved in the development of the CAOB, during the Neoproterozoic and the early, middle, and late Paleozoic eras (Safonova et al. 2017). The timing of these events was confirmed by the ages of the HP and UHP metamorphic rocks in the northern and southern parts of the CAOB (Bayarbold et al. 2022). Based on protolith compositions and typically exhumed HP and UHP rocks, oceanic plate subduction was dominant in the CAOB, but the continental subduction can explain the tectonic setting of a few HP and UHP metamorphic rocks, such as the Kokchetav massif and Muya eclogites (Zhang et al. 2012; Skuzovatov et al. 2019). Direct evidence of deep fluids in these subduction zones has been limited in the metamorphic rocks of the CAOB, except for the Kokchetav massif (De Corte et al. 1998; Hwang et al. 2006; Korsakov and Hermann 2006; Korsakov et al. 2011) and western Tianshan (Gao and Klemd 2001; Yoshida et al. 2018).

Mongolia is situated in the central part of the CAOB (Şengör et al. 1993). In western Mongolia, the Zavkhan

Terrane is bordered by the Sangelin metamorphic terrane to the north, the Neoproterozoic–early Cambrian Lake island to the west, and the Dariv metamorphic terrane to the south (Fig. 1a; Badarch et al. 2002). The Zavkhan Terrane is a single cratonic terrane (Badarch et al. 2002; Bold et al. 2016), however, Kozakov et al. (2021) identified several subzones and tectonic blocks within this terrane based on the lithological characteristics and structural patterns of the metamorphic and magmatic rocks. These subzones and blocks (from west to east) are: Zavkhan–Khungui zone, Durvuljin block, Mélange, Urgamal and Zavkhan–Mandal zones, the Erdene–Khairkhan and Bayannur blocks. The geological setting and lithological characteristics of the magmatic and metamorphic rocks in these zones and blocks are summarized by Bold et al. (2016), Kovach et al. (2021), and Kozakov et al. (2021).

The Khungui eclogite is found in the southeastern part of the Zavkhan Terrane's Mélange zone (Fig. 1b, c), and is classified into high- and low-grade rocks (Kovach et al. 2021). The high-grade rocks consist of felsic gneiss, quartzite, garnet amphibolite, and eclogite, and have been intruded by a complex of late Paleozoic alkaline intrusive rocks. The Khungui eclogite forms lenses or interlayers within the felsic gneisses and quartzites of the high-grade rocks found in the

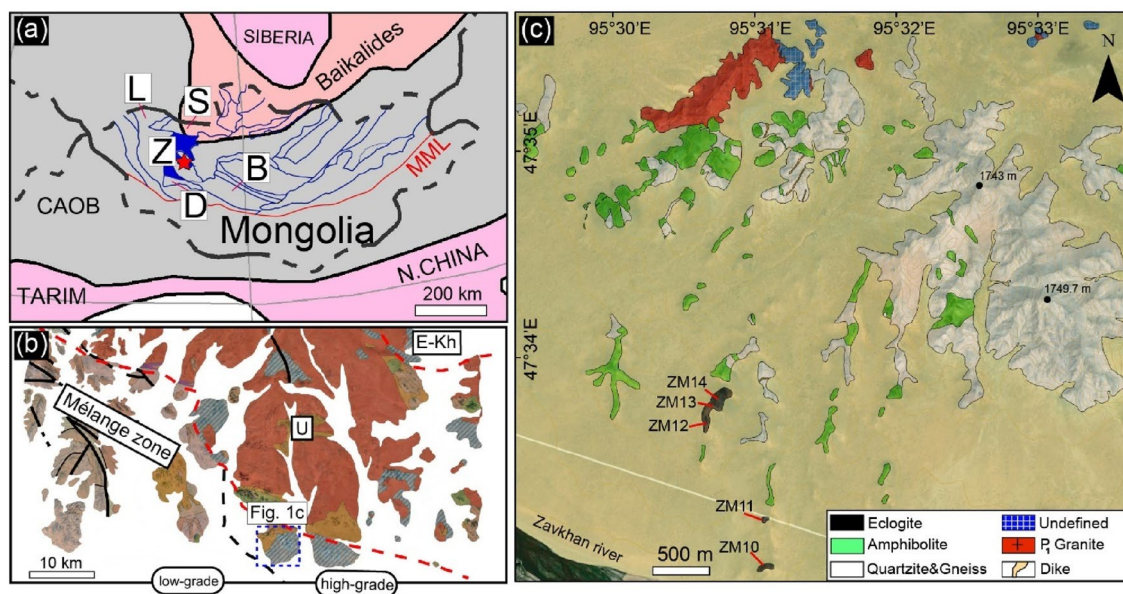


Fig. 1 a Location of the Central Asian Orogenic Belt (Şengör et al. 1993) and tectonostratigraphic terrane map of western Mongolia modified from Badarch et al. (2002). The red line represents the Mongolian Main Lineament, and the blue lines represent terrane boundaries. The red star shows the location of the study area. b Main tectonic zones of the Zavkhan Terrane (Kovach et al. 2021). The red dashed lines represent subzones boundaries in the Zavkhan Terrane, and the black dashed line shows the boundary between high- and low-grade rocks in the mélange zone. c Sample locations and geological

maps derived from satellite images of the Baruntsahir and Zuuntsahir mountains. Black circles accompanied by numbers represent the height of the mountains, and black lines accompanied by numbers indicate sampling locations. Satellite images were provided by Esri, Digital Globe, GeoEye, Earthstar Geographics, CNES/Airbus DS, USDA, USGS, AeroGRID, IGN, and the GIS User Community. Abbreviations of terrane names: L=Lake, D=Dariv, Z=Zavkhan, B=Baidrag. Subzones of the Zavkhan Terrane: U=Urgamal gneiss zone; E–Kh=Erdene–Khairkhan zone

southeastern part of the Mélange zone (Fig. 1c; Bayarbold et al. 2022).

Based on petrological studies and mineral analysis of the Khungui eclogite, Bayarbold et al. (2022) identified three metamorphic stages: (i) prograde, (ii) eclogite, and (iii) decompression. The mineral assemblage of the eclogite facies occurs as inclusions within the high-Ca rims of the garnet, and consists of omphacite, barroisite, phengite, rutile, epidote, and quartz (Fig. 2a). Based on the Cpx–Grt (Ravna 2000) and Zr-in-rutile (Tomkins et al. 2007) thermometers, and Grt–Cpx–Ph barometer (Ravna and Terry 2004), the peak pressures during metamorphism of the Khungui eclogite were estimated to be 2.1–2.2 GPa, at 580–610 °C (Bayarbold et al. 2022). Moreover, the trace element characteristics of the Khungui eclogite indicate that the protolith is a continental arc basalt, which differs from the protoliths of other HP and UHP metamorphic rocks in the CAOBS (i.e., in Mid ocean ridge basalt (MORB) and Ocean island basalt (OIB); Bayarbold et al. 2022).

Analytical methods

Electron probe micro-analysis (EPMA)

The chemical composition of the minerals in the samples were determined using an electron microprobe analyzer (EPMA; JEOL JXA-8200) at Tohoku University, Japan. The acceleration voltage used was 15 kV, beam current 12 nA, and beam diameter 1 µm. Natural and synthetic standards (wollastonite for Ca and Si, rutile for Ti, eskolaite for Cr, hematite for Fe, manganosite for Mn, periclase for Mg, albite for Na, feldspar for K, halite for Cl, and fluorite for F) were used for calibration. The counting time for the peaks and background of all the major elements were 10 and 5 s, respectively, whereas for the minor elements Cl and F they were 30 and 15 s, respectively. X-ray mapping using EPMA was conducted with an accelerating voltage of 15 kV, beam current 120 nA, dwell time 150–200 ms, and beam diameter 1 µm.

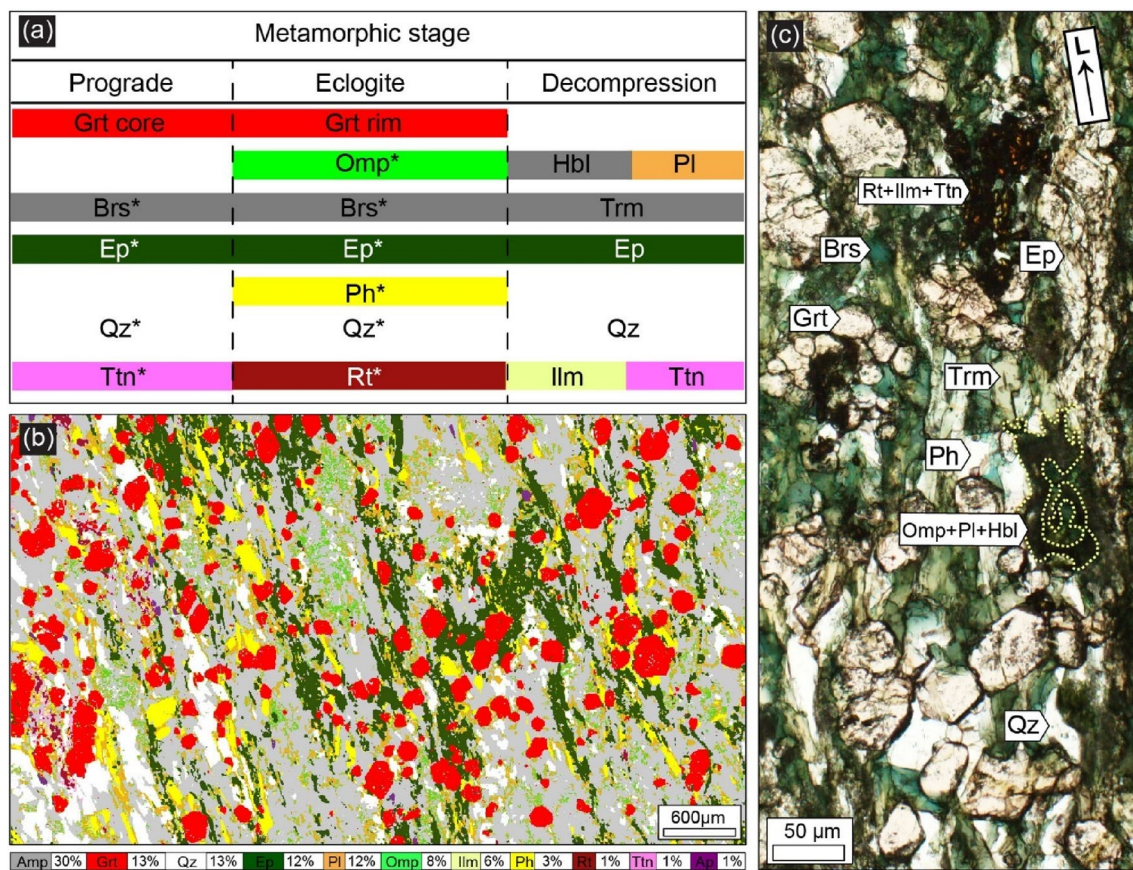


Fig. 2 **a** Metamorphic evolution of the Khungui eclogite (modified from Bayarbold et al. 2022). **b** Modal map of sample ZM10 obtained from processing an electron probe micro elemental map (Lanari et al. 2014). **c** Photomicrograph of sample ZM10. Mineral abbreviations (as per Whitney and Evans 2010): garnet (Grt), epidote (Ep), bar-

roisite (Brs), taramite (Trm), phengite (Ph), omphacite (Omp), plagioclase (Pl), hornblende (Hbl), quartz (Qz), rutile (Rt), ilmenite (Ilm), and titanite (Ttn). (*) indicates minerals that occur from both inclusions in the garnet and matrix of the studied sample

Fluid inclusion microthermometry

A doubly polished thick section (~ 100 μm thick) of the Khungui eclogite sample was prepared for fluid inclusion analysis. Microthermometry was performed at Tohoku University using a Linkam THMS600 heating/freezing stage, with an operating temperature range of -180 to 600 $^{\circ}\text{C}$. The homogenization and ice melting temperatures were determined at a heating rate of 1 $^{\circ}\text{C}/\text{min}$ and 0.2 $^{\circ}\text{C}/\text{min}$, respectively. The salinity of the fluid inclusions was measured in NaCl wt.% equivalent (eq.) using the final melting temperature of ice (Bodnar 1993). The fluid inclusion isochores were determined using the equation described by Bodnar (2003).

Combined FIB and X-ray CT analysis

To determine the volume proportion of each phase, high-resolution three-dimensional images of multiphase-solid fluid inclusion in garnet were obtained using Synchrotron radiation nanoscopic X-ray CT (SR-XCT). A small particle containing fluid inclusion was selected from a thin section of the eclogite sample, for SR-XCT observation using a scanning electron microscope (SEM) with a focused ion beam (FIB), as described by Yoshida et al. (2016). A specific area of the sample (20×20 μm^2) was cut out to depth of 20 μm and held at the tip of a tungsten needle. The FIB analysis was performed using a Helios NanoLab G4 system (Thermo Scientific) at the Japan Agency for Marine-Earth Science and Technology (JAMSTEC), Japan. The analyses employed a Ga^+ gun at 30 kV voltage and 0.09 – 20 nA current.

SR-XCT measurements were performed on the NW2A beamline of the Photon Factory Advanced Ring Synchrotron facility at the Institute of Materials Structure Science, High Energy Accelerator Research Organization (KEK), Japan (Niwa et al. 2019). The voxel size and X-ray beam energy were maintained at 24.2 nm and 7118 eV, respectively. The X-ray CT measurements were performed by rotating the test stage (-90° to 90°). Consequently, 1441 radiographs were obtained with an exposure time of 2 s (total scan time of approximately 1 h).

FIB–SEM analysis provides the opportunity to directly analyze the coexisting solid phases in a fluid inclusion by excavating the inclusions (Yoshida et al. 2018). After the SR-XCT observations, the composition of the solid phases in the multiphase-solid fluid inclusion was determined using Energy-Dispersive X-ray Spectrometry (EDS). The micro-sample held on the tungsten needle was machined using the FIB system at 30 kV voltage and 9.1 nA current until the multiphase-solid fluid inclusion reached the surface. The EDS analysis was performed at an acceleration voltage of 15 kV and beam current of 1.6 nA. The X-ray spectra were measured such that the exposed surface became horizontal.

Microanalysis using Raman spectroscopy

Raman spectroscopy was used to identify the fluids and solids in the garnet and quartz inclusions. The analyses were performed using a HORIBA XploRA Plus Confocal Raman Microscope at the Graduate School of Environmental Studies, Tohoku University, Japan. The laser beam was positioned using a built-in Olympus BX optical polarizing microscope. The spectrum acquired after excitation with a 532 nm solid-state wavelength was measured with a CCD detector cooled to -70 $^{\circ}\text{C}$ by a Peltier cooling system. The analyses were performed in a backscattered geometry, and the scattered light was focused using a $100\times$ lens. The spectra were obtained in the range of 100 – 4200 cm^{-1} . The spectrometer was calibrated using a pure silicon line (520.7 cm^{-1}) and an intrinsic laser line (0 cm^{-1}). The spectral resolution of the diffraction grating was 1800 g/mm. Measurements were carried out with 100 – 300 μm apertures. The counting time and number of counting cycles within a spectral window varied from five cycles of 5 s to twenty cycles of 20 s. Detailed analytical condition of 2D Raman mapping is mentioned in Table S1. The scanning step was set at 0.5×0.5 μm . The exposure time was set to 3 s, with three acquisitions per point.

Petrography and mineralogy of the eclogite samples

Petrography

Five eclogite samples are analyzed; the mineral assemblages of the samples are presented in Table 1. The mineral abbreviations used in this study are obtained from Whitney and Evans (2010). The composition of the main minerals of the Khungui eclogite has already been documented (Bayarbold et al. 2022). Therefore, we focus our study on fluid inclusion-hosted minerals and minerals found in fluid inclusions. All chemical and representative microprobe data for the minerals are listed in Table 2.

All the eclogite samples analyzed are partly affected by retrograde metamorphism, resulting in a symplectite texture of hornblende and plagioclase replacing omphacite. As all eclogite samples show similar mineralogical characteristics, we present the results of our mineralogical analysis for one representative sample. Foliation and lineation are well defined by the elongated texture of quartz, Ti-bearing minerals, and phengite in the matrix (Fig. 2b, c). Volume percent (vol. %) of mineral assemblage in this representative eclogite is found to be: amphibole (30%), garnet (13%), quartz (13%), epidote (12%), plagioclase (12%), omphacite (8%), Ti-bearing minerals (ilmenite–6%, rutile–1%, and titanite–1%), and phengite (3%),

Table 1 Modal abundance of minerals and fluid inclusions (FI) in the Khungui eclogite

Matrix mineral assemblages (in vol.%)														Host mineral of FI	
Samples	Grt**	Omp**	Amp**	Ph**	Ep**	Pl	Qz**	Rt**	Ttn	Ilm	Zrn	Ap	Grt	Qz	
ZM10*	13%	8%	30%	3%	12%	12%	13%	6%	1%	1%	+	+	+	+	
ZM11	+	+	+	+	+	+	+	+	+	+	+		+		
ZM12	+	+	+	+	+	+	+	+	+	+					
ZM13	+	+	+	+	+	+	+	+	+	+	+				
ZM14	+	+	+	+	+	+	+	+	+	+				+	
Inclusion minerals in Grt															
Grt-core			+		+		+		+						
Grt-rim		+	+	+	+			+				+			
Solid phases in the multiphase-solid fluid inclusions in Grt (in vol. %)															
No	Qz	Cal	Amp	Ap	Mica	HI	Chl	L	V	void					
1		13	18		20			37	12						
2		23	41			1		24	12						
3		26				5		48	20						
4		3	19		8	2	14	35	18						
5	52	11	19			1		11	6						
6	27							52	21						
7	74							21	4						
8 [#]			44	33	9					14					

The sample with an asterisk (*) was analyzed using Raman spectroscopy and microthermometry experiments. Mineral names with double asterisks (**) represent the eclogite facies mineral assemblage of the Khungui eclogite. ([#]) Surfaced inclusion observed in EPMA. Void was observed and interpreted as former liquid and vapor. *Grt*, garnet, *Omp* omphacite, *Amp* amphibole, *Ph* phengite, *Ep* epidote, *Pl* plagioclase, *Qz* quartz, *Rt* rutile, *Ttn* titanite, *Ilm* ilmenite, *Zrn* zircon, *Ap* apatite, *Chl* chlorite, *Cal* calcite, *HI* halite, *L* liquid; *V* vapor

with small amounts (< 1%) of K-feldspar, calcite, chlorite, apatite, and zircon (Fig. 2b; Bayarbold et al. 2022).

Garnet

Garnet (Grt) occurs as euhedral crystals (> 100 μm) and aggregates (> 500 μm) of crystals (Fig. 2b). The euhedral Grt crystals show symmetrical compositional zoning, with the grossular (Grs) content increasing continuously from core to rim, while the almandine (Alm), pyrope (Prp), and spessartine (Sps) contents decrease (Fig. 3a, b). The range of composition in the euhedral Grt cores are: Alm, 61–66%; Grs, 22–27%; Prp, 9–10%; Sps, 3–4%; and in the Grt rims are: Alm, 58–61%, Grs, 31–35%; Prp, 5–8%; Sps, 1–3%. Moreover, the euhedral Grt crystals show zoning of trace elements such as Ti; the characteristic of Ti zoning was similar to Ca zoning (Fig. 3a). The core and rim compositions of the euhedral Grt crystals can be clearly distinguished by their Mg, Ca, and Fe euhedral compositional zones (Fig. 3a, b, e).

Garnet inclusions

The high-Ca Grt rims mainly contain inclusions of rutile (Rt), omphacite (Omp), epidote (Ep), amphibole (Amp), and quartz (Qz), and rarely apatite (Ap), and phengite (Ph) (Fig. 3a and g); whereas the main inclusions in the Ca-poor cores are Ep, Qz, Amp and titanite (Ttn) (Figs. 2a, 3a, g, and 4a; Table 1). Moreover, the euhedral crystals of Grt also contain bi-phase fluid inclusions (liquid and vapor) and the multiphase-solid fluid inclusions (liquid, vapor, and several solid phases) (Figs. 3a, e, 4).

Quartz

The Qz occurs with various grain sizes (10–200 μm) in the matrix and as inclusions (5–10 μm) in Grt, Omp, and Ap (Figs. 2c, 4a). In addition, the variably sized anhedral and subhedral Qz grains in the matrix has highly irregular interpenetrating boundaries (Fig. S1d). The Qz matrix grains contain rare inclusions of zircon, rutile, and apatite.

Table 2 Representative electron microprobe analyses of the matrix, inclusion minerals in garnet, and some solid-phase particles exposed in multiphase-solid fluid inclusion in the studied sample

Mineral	Grt-c	Grt-r	Amp-c-in-Grt	Amp-r-in-Grt	Rt-matrix	Rt-in-Grt	Ap-c-matrix	Ap-r-matrix	Bt	Act	Ap	Chl *
SiO ₂	37.76	38.20	43.98	42.90	0.01	nd	0.25	0.08	35.29	49.56	0.01	29.02
TiO ₂	0.09	0.13	0.26	0.22	99.14	98.2	0.05	nd	0.4	0.06	nd	nd
Al ₂ O ₃	21.41	21.40	13.43	14.49	0.01	nd	0.02	nd	15.15	4.12	0.02	26.81
FeOT	28.83	26.60	19.10	20.09	0.32	0.8	0.11	0.40	23.07	17.29	0.83	38.28
MnO	1.7	0.5	0.09	0.05	nd	nd	0.02	0.08	0.29	0.36	nd	nd
MgO	2.36	1.74	6.72	6.08	nd	nd	0.02	0.03	7.24	11.22	0.02	3.79
CaO	7.57	11.74	8.03	7.78	nd	0.3	56.17	56.49	0.38	12.22	56.08	2.10
Na ₂ O	0.09	nd	3.77	4.68	nd	0.1	nd	nd	nd	0.43	nd	nd
K ₂ O	nd	nd	0.42	0.27	nd	nd	0.01	nd	8.75	0.19	nd	nd
P ₂ O ₅	nd	nd	nd	nd	nd	nd	41.73	40.48	nd	nd	42.27	nd
Cl	nd	nd	0.07	1.01	nd	nd	0.10	0.12	0.43	0.08	0.25	nd
F	nd	nd	nd	nd	nd	nd	2.27	2.37	nd	nd	1.32	nd
Total	99.8	100.3	95.9	97.6	99.5	99.4	100.7	100.0	91.0	95.5	100.2	100.00
O	12	12	23	23					11	23		
Si	3.01	3.01	6.63	6.52					2.84	7.37		
Ti	0.01	0.01	0.00	0.00					0.04	0.00		
Al	2.01	1.99	2.38	2.59					1.44	0.72		
Fe ³⁺	0.00	0.00	0.40	0.27					0.55	0.37		
Fe ²⁺	1.92	1.75	2.00	2.28					1.01	1.92		
Mn	0.11	0.03	0.02	0.02					0.02	0.04		
Mg	0.28	0.20	1.51	1.38					1.02	2.49		
Ca	0.65	0.99	1.32	1.30					0.03	1.96		
Na	0.01	0.00	1.10	1.39					0.00	0.17		
K	0.00	0.00	0.08	0.07					0.83	0.04		
Cl			0.02	0.26					0.06	0.02		
X (phase)	0.22	0.33	0.57	0.62	–	–	–	–	–	0.44	–	–
Y (phase)	0.65	0.59	0.14	0.09	–	–	–	–	–	0.34	–	–

The electron microprobe analytical data were calculated using the AX_2 program (Holland; <http://www.esc.cam.ac.uk/research-groups/holland/ax/>): $X(\text{grt}) = \text{Ca}/(\text{Fe}^{2+} + \text{Mn} + \text{Mg} + \text{Ca})$, $X(\text{amp}) = \text{Fe}^{2+}/(\text{Fe}^{2+} + \text{Mg})$, $Y(\text{grt}) = \text{Fe}^{2+}/(\text{Fe}^{2+} + \text{Mn} + \text{Mg} + \text{Ca})$, $Y(\text{amp}) = \text{Fe}^{3+}/(\text{Fe}^{3+} + \text{Al})$. Abbreviations: c, core; m, mantle; r, rim; in, inclusion; nd., not detected. (*) represents the semi-quantitative composition of the mineral, as determined by the FIB–SEM–EDS analysis

Amphibole

The matrix Amp shows compositional zoning, with barroisite (Brs) in the core and taramite (Trm) in the rim (Figs. 2c, 4c). Brs also occurs as inclusions in the Grt rims, and rarely in the Grt cores (Figs. 2a, 3a, c, d, g, 4a). The Brs inclusions show zoning of Mg, Cl, and Al; the Mg content decreased from core to rim (6.72–6.08 wt. %, MgO), whereas the Al (13.43–14.49 wt. %, Al₂O₃) and Cl (0.07–1.01 wt. %, of the pure element) contents increase (Fig. 3a, c, d; Table 2). Amp in the symplectitic intergrowths with plagioclase (Pl) is hornblende (Hbl) (Fig. 2c, 4c). The Cl content of the Amp matrix (Brs, Trm, and Hbl) is below the detection limit. Amp also occurs in the multiphase-solid fluid inclusions in Grt, and is composed of actinolite (Act) (Fig. 4b, c). The Cl content in Act (0.08 wt. %) is similar to that of the core of Brs inclusions (Table 2).

Ti-bearing minerals

The primary Ti-bearing minerals are Rt, ilmenite (Ilm), and titanite (Ttn). These minerals occur together in the matrix, whereas only Rt and Ttn occur as inclusions in the Ca-rich rims and Ca-poor cores of the Grt, respectively (Figs. 3a, 4a). In the matrix, Rt is commonly surrounded or overlapped by Ilm and Ttn; however, the order of crystallization is unclear in some instances (Fig. S2a). The Rt in the matrix contains inclusions of zircon (Zr) and Ttn.

Apatite

The Ap occurs in the matrix and as inclusions in Grt. The Ap in the matrix is subhedral with a grain size of 50 μm, which commonly occurs with Ti-bearing minerals (Fig. S2a). In addition, Ap shows a compositional zoning in Cl, which is

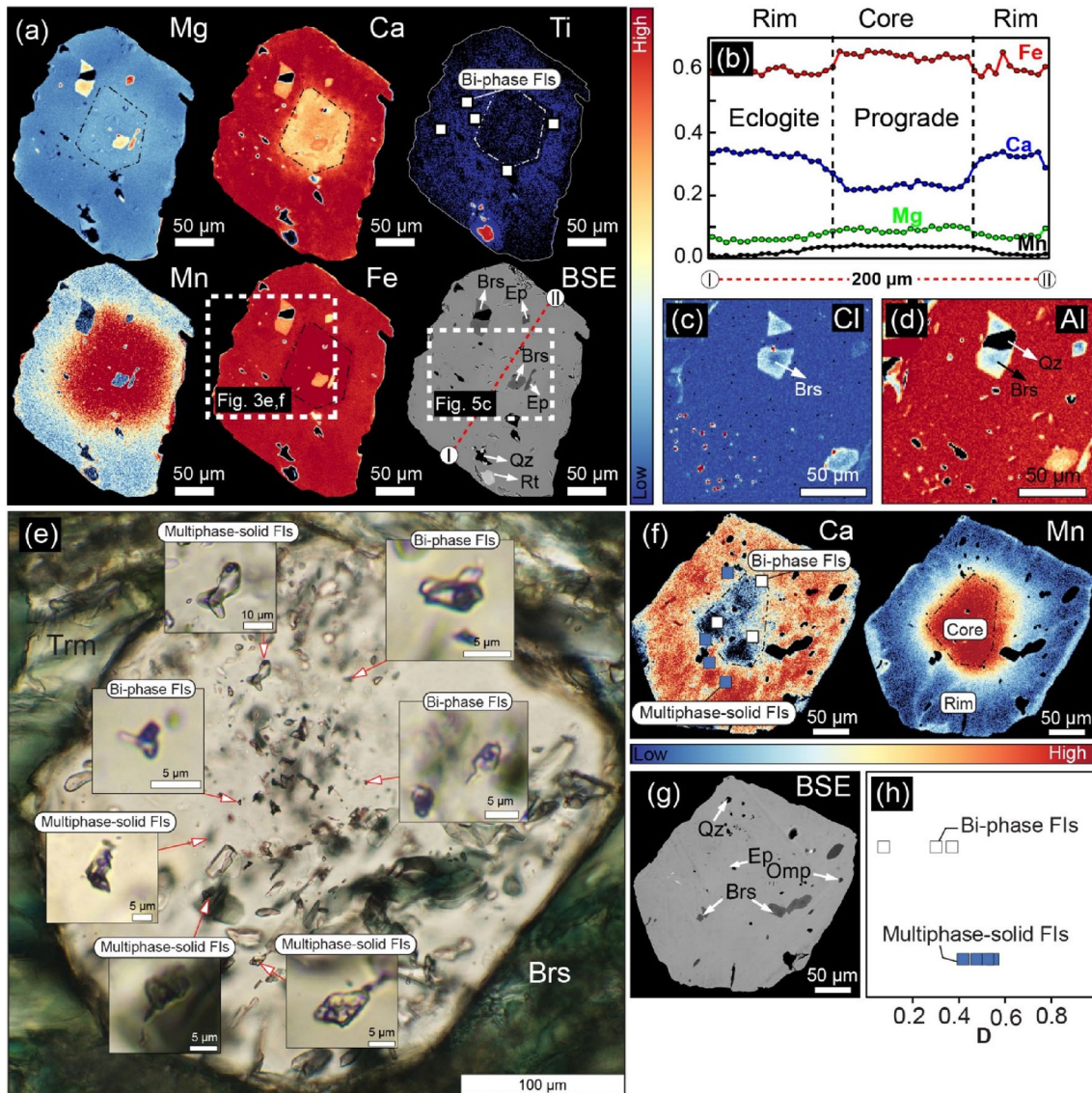


Fig. 3 X-ray element mapping of garnet and fluid inclusions. **a** Element (Mg, Ca, Ti, Mn, and Fe) maps and backscattered electron image of the garnet. White boxes indicate the location of fluid inclusions in the garnet. Black and white dotted lines show the border of the core and rim of the garnet. The red line on the backscattered electron image shows the position of the garnet composition profile given in (b). **b** Composition profile across the center of the studied garnet (Fe, Ca, Mg, and Mn). The black dashed lines separate the garnet

compositions of the prograde and eclogite facies metamorphic stages. **c** Cl and **d** Al element mapping of an inclusion of amphibole (Brs) in garnet. Note: All element maps are optimized for maximum contrast to highlight compositional features. **e** Photomicrograph of single garnet shows the systematic distribution of primary bi-phase and multiphase-solid fluid inclusions. **f** Ca and Mg elemental maps and **g** BSE images of the garnet in **e**. **h** Systematic distribution of bi-phase and multiphase-solid fluid inclusion in garnet

characterized in the matrix by an increased amount from the core (Cl=0.10 wt. %) to the rim (Cl=0.12 wt. %) (Table 2; Fig. S2b). Inclusions of Ap commonly occurs with Omp in the Ca-rich rims of Grt (Fig. S2b). Ap (Cl=0.25 wt.%) also occurs within the exposed multiphase-solid fluid inclusions in the Grt (Fig. 4b). The Cl content of Ap varies with its occurrence; for example, matrix Ap has a much lower Cl content (0.10–0.12 wt. %) than the Ap inclusions in Grt (0.25 wt. %) (Table 2).

Characteristics of fluid inclusions

Detailed analysis of one eclogite sample (ZM10) reveals various types of fluid inclusions (FIs) in both Grt and Qz (Fig. 5; Table 1); however, the other key minerals (Omp, Amp, and Pl) of the Khungui eclogite do not contain FIs.

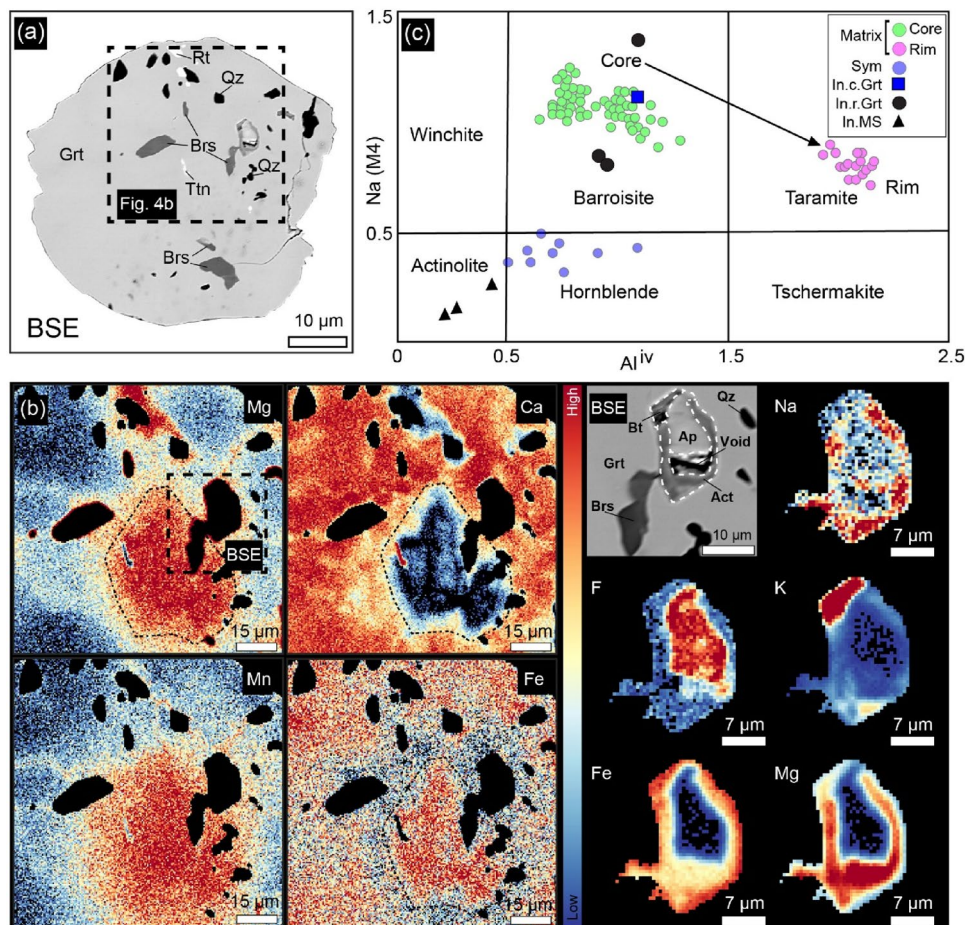


Fig. 4 The exposed multiphase-solid fluid inclusion in garnet. **a** Backscattered electron image of the euhedral garnet and included minerals. **b** Four element maps (Mg, Ca, Fe, and Mn) of the garnet (excluding other minerals) and backscattered electron image with five element maps (Na, F, K, Fe, and Mg) for the exposed multiphase-solid fluid inclusion. Black dotted lines indicate the border of the core and rim of the garnet. White dashed line presents boundary of solid phases. **c** Na (M4 site) vs Al (T site) diagram for amphiboles. The matrix amphibole composition used was cited from Bayarbold

et al. (2022). The core and rim compositions of the matrix amphibole are represented by green and pink circles, respectively. Blue circles show amphibole compositions in the symplectites (Sym). Black circles show composition of amphibole inclusion in the garnet rim (In.r.Grt), whereas blue square presents composition in the garnet core (In.c.Grt). Black triangles represent amphibole compositions in the multiphase-solid fluid inclusion (In.MS). Note: All element maps are optimized for maximum contrast to highlight compositional features

Fluid inclusions in quartz

The Qz grains in the matrix contain both primary and secondary FIs. The primary FIs (< 5 μm) in matrix Qz consist of an aqueous solution, vapor, and rarely halite (HI) crystals (Fig. 5a). HI crystals mostly occur in irregularly shaped primary FIs, whereas the HI-free primary FIs in Qz had ellipsoidal shapes (Fig. 5a). Analyses of the photomicrographs (Fig. 5a) reveal that the HI-bearing primary FIs in Qz are composed of 3 vol. % vapor, 20 vol. % HI, and 77 vol. % liquid; the HI-free primary FIs are composed of 10–19 vol. % vapor, and 81–90 vol. % liquid.

Secondary FIs in Qz are subdivided into two types based on their occurrence. Type I secondary FIs are aligned along the healed cracks with random orientations

and consist of two phases at room temperature: a vapor and an aqueous solution (Fig. 5a). Type II secondary FIs occur in close association with micro-vein (20–50 μm wide) is composed of K-feldspar (Kfs) and calcite (Cal). The micro-vein (Kfs + Cal) intersects the matrix minerals such as Grt, Omp, Amp, and Qz (Fig. S1a, c). Type II secondary FIs are aligned at low angles to the micro-veins (Fig. S1b) and composes of liquid and vapor phases. The sizes of primary and secondary FIs in the Qz varies from 1 to 4 μm.

Raman spectroscopy shows that the liquid parts of the FIs in Qz exhibit a broad peak in the range of 3100–3600 cm⁻¹, indicating the presence of H₂O. Peaks corresponding to gases such as CO₂ and CH₄ are not detected in the vapors from the HI-free primary FIs and Type I and Type II

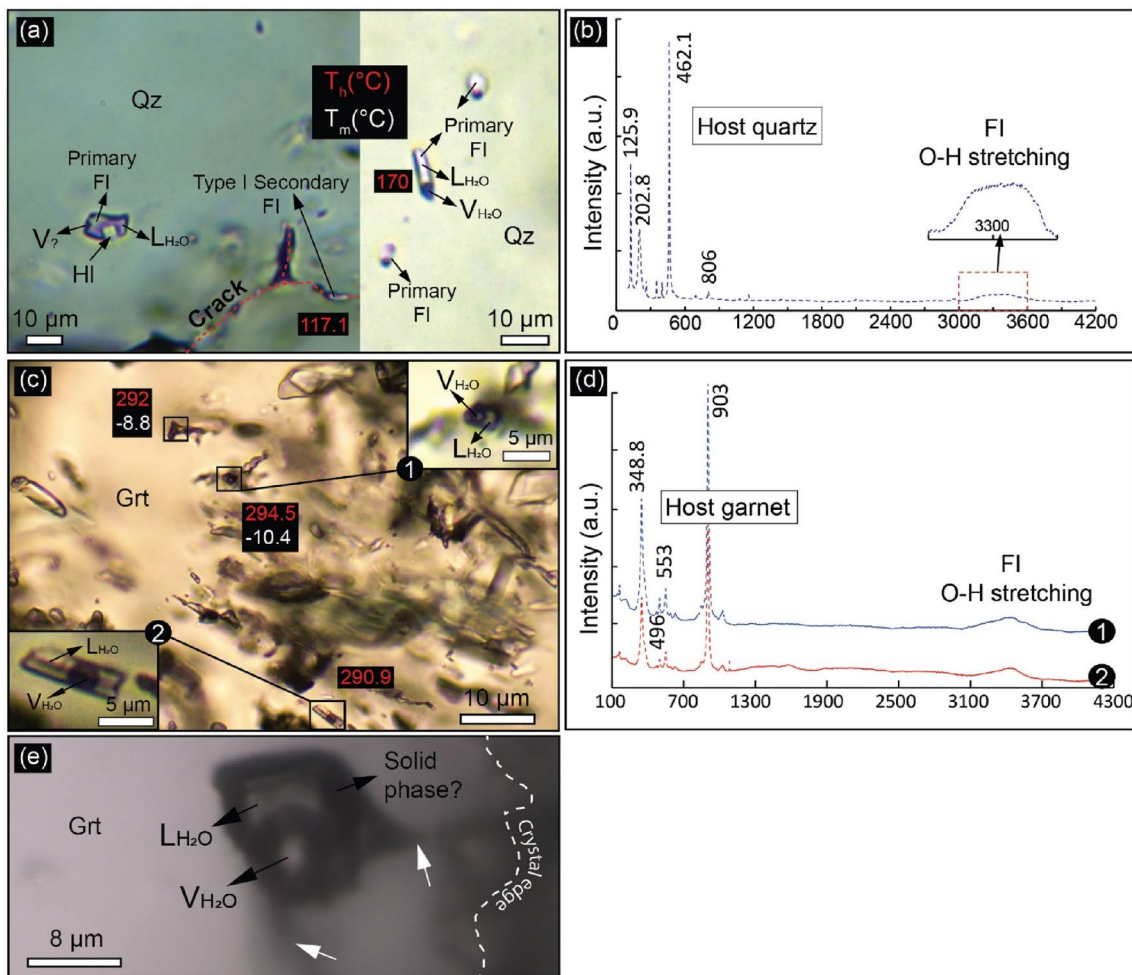


Fig. 5 **a** Primary/secondary fluid inclusions in quartz. **b** Representative Raman spectra for a mixed primary fluid inclusion in quartz. **c** Primary bi-phase fluid inclusion in garnet. **d** Representative Raman spectra for mixed primary bi-phase fluid inclusion in garnet. **e** Representa-

representative of irregular-shaped primary multiphase-solid fluid inclusion in garnet. White arrows show microcracks. L_{H_2O} liquid water, V_{H_2O} vapor water, HI halite, FI fluid inclusion, $T_h(^{\circ}C)$ homogenization temperature, $T_m(^{\circ}C)$ ice melting temperature

secondary FI in Qz (Fig. 5b). Detecting the vapor within HI-bearing FI in Qz using Raman spectroscopy is difficult to determine due to its tiny size ($<0.5 \mu m$). Therefore, it is still uncertain whether vapor hosts gas phases or not (Fig. 5a).

Fluid inclusions in garnet

The Grt crystals contain only primary FIs; these primary FIs are classified into two types: bi-phase and multiphase-solid FIs. The most common primary FIs in Grt are bi-phase FIs ($1.5\text{--}5.5 \mu m$), which contain a vapor and an aqueous fluid without minerals (Figs. 3e, 5c; Table 3). Multiphase-solid FIs are relatively rare, typically larger than $9 \mu m$ (Figs. 3e, 5e, 6; Table 3), and show irregular shapes; they contain a vapor and an aqueous liquid with several solid phases (Figs. 6 and 7). No other volatile compounds (N_2 , CO_2 , or CH_4) are detected in either the bi-phase or multiphase-solid

FIs of Grt. The bi-phase FIs ($D=0.07\text{--}0.37$) are presented in both the Ca-poor Grt core and the inner part of the Ca-rich Grt rim, whereas the multiphase-solid FIs ($D=0.42\text{--}0.53$) are preferentially observed at the outer part of the Ca-rich Grt rim (Figs. 3e, f, h; Fig. S3). ‘D’ is the normalized value of the absolute distance between the center and crystal edge of Grt.

The vol. % for the vapor and liquid phases in the bi-phase FI are estimated to be 9.7–22.1% and 77.9–90.3%, respectively. Moreover, the bi-phase FIs exhibit tubular shapes (Figs. 3e and 5c).

The results of Raman spectroscopy and FIB–SEM analyses indicate that the solid phases in the primary multiphase-solid FIs in Grt include mica, Cal, Amp, Qz, chlorite (Chl), Ap, and rarely HI (Figs. 6 and 7; Table 1; Fig. S4). Cal shows strong Raman peaks at 1085 , 278 , and 710 cm^{-1} ; mica at 195 , 209 , 262 , 403 , 701 , 3620 , and 3654 cm^{-1} ; and Amp

Table 3 Measured ice melting temperatures (T_{mt}), homogenization temperatures of liquid (T_{hV-L}), and calculated salinities of FI minerals

Mineral	Fluid inclusion	Salinity, NaCl wt. % eq	T_{mt} (°C)	T_{hV-L} (°C)	Size (μm)	Eutectic temperature	Fluid system
FI/Qz-1	Primary	15.9	- 11.9	136.7	1.54		
FI/Qz-2	Primary	15.9	- 11.9	141.1	1.3		
FI/Qz-3	Primary	-	nd	139.5	2		
FI/Qz-4	Primary	15.9	- 11.9	141.1	2		
FI/Qz-5	Primary	16.4	- 12.5	174	1.13	- 32.8	MgCl ₂ -H ₂ O
FI/Qz-6	Primary	15.7	- 11.7	170.4	1.34	- 32.8	MgCl ₂ -H ₂ O
FI/Qz-7	Primary	16.2	- 12.3	173.5	1.9	- 32.8	MgCl ₂ -H ₂ O
FI/Qz-8	Primary	-	nd	196.4	1.77		
FI/Qz-9	Primary	-	nd	174	1.65		
FI/Qz-10	Primary	-	nd	170	2.3		
FI/Qz-11	Primary	-	nd	168	2		
FI/Qz-12	Primary	-	nd	172	2.2		
FI/Qz-13	Primary	-	nd	156	2.6		
FI/Qz-14	Primary	-	nd	153	2.7		
FI/Qz-15	Primary	-	nd	174	3.2		
FI/Qz-16	Primary	-	nd	168	1.9		
FI/Qz-1	Type I secondary	12.6	- 8.8	139	1.38		
FI/Qz-2	Type I secondary	-	nd	117.1	1.32		
FI/Qz-3	Type I secondary	12.5	- 8.7	181.5	1.3		
FI/Qz-4	Type I secondary	-	nd	181.5	1.75		
FI/Qz-5	Type I secondary	-	nd	150	1.5		
FI/Qz-6	Type I secondary	14.04	- 10.1	nd	2.9		
FI/Qz-7	Type I secondary	14.77	- 10.8	nd	2.4		
FI/Qz-8	Type I secondary	13.51	- 9.6	nd	3.7		
FI/Qz-9	Type I secondary	14.67	- 10.7	nd	2.5		
FI/Qz-10	Type I secondary	16.34	- 12.4	nd	4.4		
FI/Qz-11	Type II secondary	6.74	- 4.2	nd	2.9		
FI/Qz-12	Type II secondary	7.17	- 4.5	nd	3.2	- 36	(Fe ± Mg)Cl ₂ -H ₂ O
FI/Qz-13	Type II secondary	6.45	- 4	nd	2.7		
FI/Qz-14	Type II secondary	6.88	- 4.3	nd	3.3		
FI/Qz-15	Type II secondary	10.61	- 7.1	nd	3.2		
FI/Grt-1	Multi-phase	12.9	- 9	270	9.1		
FI/Grt-2	Multi-phase	-	nd	303.4	9.2		
FI/Grt-3	bi-phase	-	nd	306.8	3.4		
FI/Grt-4	bi-phase	-	nd	318.5	2.2		
FI/Grt-5	bi-phase	-	nd	290.9	2.7		
FI/Grt-6	bi-phase	14.4	- 10.4	294.5	1.6		
FI/Grt-7	bi-phase	-	nd	298	2.2		
FI/Grt-8	bi-phase	-	nd	297.6	2.5		
FI/Grt-9	bi-phase	13.7	- 10.2	303.5	5.3	- 37.8	MgCl ₂ -KCl-H ₂ O
FI/Grt-10	bi-phase	16.15	- 12.2	299.4	3.2		
FI/Grt-11	bi-phase	-	nd	230.9	2.1		
FI/Grt-12	bi-phase	13.07	- 9.2	303.5	5.0		
FI/Grt-13	bi-phase	-	nd	327.5	3.5		

Salinity was estimated using the method described by Bodnar (1993). *nd* not detected, -, did not calculate. All ice-melting temperatures were estimated from the HI-free fluid inclusions

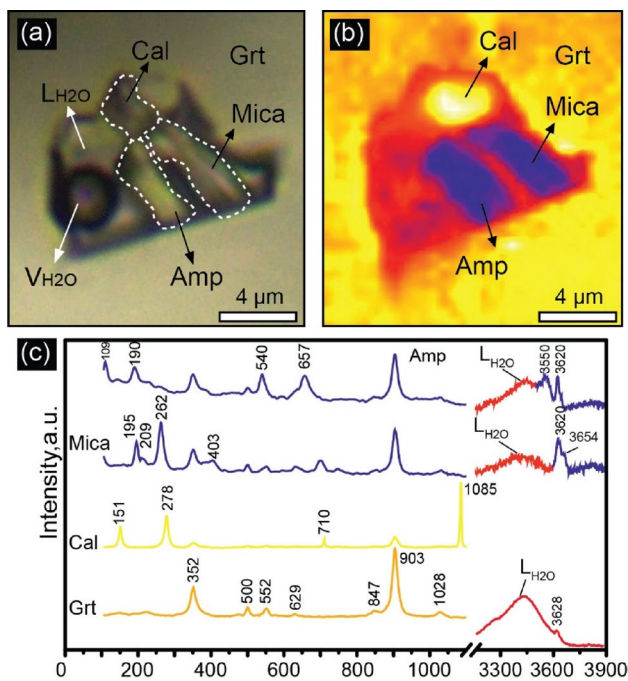


Fig. 6 2D observation of a multiphase-solid fluid inclusion in garnet. **a** Photomicrograph of the multiphase-solid fluid inclusion in the garnet (cross polarized light). **b** Distribution of different phases within the fluid inclusion, based on the detailed Raman image. **c** Raman spectra for each phase of the multiphase-solid fluid inclusion in garnet. L_{H_2O} pure water, V_{H_2O} water vapor, *Amp* amphibole, *Cal* calcite, *Grt* garnet

at 190, 540, 657, and 3552 cm^{-1} (Fig. 6c; Li et al. 2011), although detailed identification of mica and *Amp* species are difficult because of their small sizes. In rare cases, primary multiphase-solid FIs are exposed at the surface of thin sections, along with the minerals biotite (*Bt*), *Act*, *Ap*, and voids (Fig. 4a–b) that are identified using EPMA (Table 2). *Chl* composition is estimated using FIB–SEM–EDS analysis. *Bt*, *Act*, *Chl*, and *Cal* crystals are observed along the walls of the host *Grt* (Figs. 4b, 6a–b, 7). Some multiphase-solid FIs exhibit irregular shapes surrounded by microcracks (Figs. 5e, 7b).

Vol. % of the liquid, vapor, and minerals of multiphase-solid FIs are roughly estimated using a 2D photomicrographs and Raman images: 27–74% *Qz*; 3–26% *Cal*, 18–44% *Amp*, 8–20% mica, 1–5% *HI*, 11–52% liquid, and 4–21% vapor (Fig. S4; Table 1).

The detailed microstructures of the solid phases in the multiphase-solid FI in *Grt* are analyzed using SR-XCT images (Fig. 7c). *Chl* and *Cal* occur as anhedral crystals along the walls of the host *Grt*. Moreover, the anhedral crystal of *Cal* in FI is entirely covered by *Chl*. *Amp* appears as subhedral rectangular crystals, whereas mica appears as subhedral flakes. The *HI*, which occurs as well-shaped cuboids, is limited to the walls of the FI (Fig. 7). The precise vol. % of

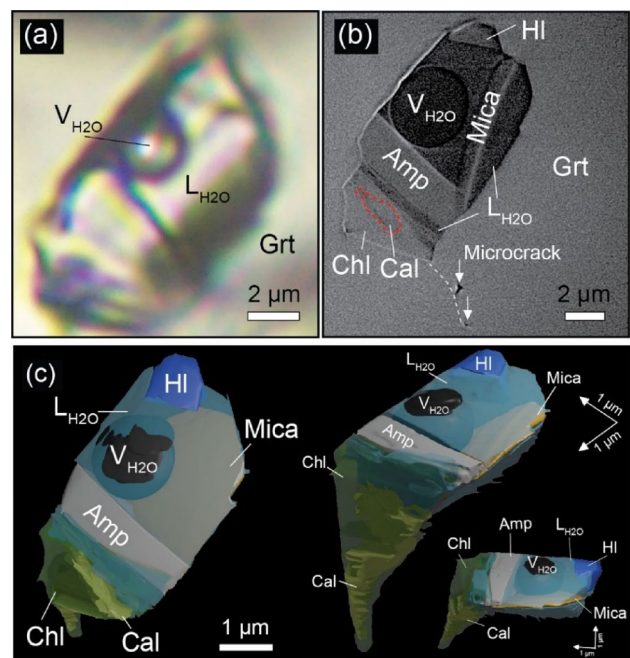


Fig. 7 3D observations of a representative multiphase-solid fluid inclusion in garnet. **a** Photomicrograph of the multiphase-solid fluid inclusion in garnet (cross polarized light). **b** Distribution of different phases within the fluid inclusion, shown in a single cross-section of the SR-XCT 3D image. White arrows indicate microcracks. **c** 3D model of the multiphase-solid fluid inclusion in garnet, based on synchrotron SR-XCT data. L_{H_2O} liquid water, V_{H_2O} vapor water, *HI* halite, *Amp* amphibole, *Chl* chlorite, *Cal* calcite, *Grt* garnet

mica, *Cal*, *HI*, *Amp*, *Chl*, liquid, and vapor are found to be 4% ($15\text{ }\mu\text{m}^3$), 6% ($22\text{ }\mu\text{m}^3$), 7% ($25\text{ }\mu\text{m}^3$), 16% ($56\text{ }\mu\text{m}^3$), 16% ($56\text{ }\mu\text{m}^3$), 38% ($134\text{ }\mu\text{m}^3$), and 12% ($42\text{ }\mu\text{m}^3$), respectively (Fig. 7c; Table 4).

Microthermometry

Microthermometry is performed on *HI*-free primary and secondary FIs in *Qz* and primary FIs in *Grt* (Table 3). However, the amount of microthermometric data obtained in this study is limited by: (1) the small size of the common FIs (most FIs are smaller than $5\text{ }\mu\text{m}$) and (2) the appearance of large solid phases along with fluids in the inclusions.

Fluid inclusions in quartz

Most primary FIs and all secondary FIs in *Qz* contain two phases, liquid, and vapor, at room temperature (Fig. 5a; Fig. S1). The ice melting temperature (T_{mt}) of the primary FIs in *Qz* ranged from -11.7 to $-12.5\text{ }^\circ\text{C}$, corresponding to a salinity of 15.7–16.4 wt. % *NaCl* eq. (Fig. 8a; Table 3). The rare primary FIs in *Qz* include cubic *HI* crystals (Fig. 5a), indicating that the salinity of the primary FI is higher than

Table 4 Estimated vol. % of all solid phases in a primary multiphase-solid fluid inclusion (MS. FI) in garnet and fluid compositions estimated by mass balance (in molal)

Volume % estimated of solid phases in MS. FI		
Observation	3D	2D
Cal	6	3
Amp	16	19
Bt	4	8
Hl	7	2
Chl	16	14
L _{H2O}	38	35
V _{H2O}	12	18
Tot. S	50	46
Tot. L	38	35
Tot. V	12	18
S/F	0.5	0.4
Estimated composition of initial fluid (molal)		
Si	0.0	0.0
Ti	0.0	0.1
Al	0.0	0.0
Fe	2.9	3.4
Mn	0.0	0.1
Mg	2.1	2.3
Ca	2.7	0.7
Na	10.4	3.1
K	0.5	1.1
Cl	12.7	7.0
C	3.8	1.5
Weight percent (wt.%)		
H ₂ O	43.3	55.9
NaCl	32.2	22.8
X _{NaCl}	0.18	0.11
X _{CO2}	0.05	0.02

The solid-to-fluid ratio is defined as $S/F = \text{Tot. S.} / (\text{Tot. S.} + \text{Tot. L.} + \text{Tot. V.})$. $X_{\text{NaCl}} [= \text{NaCl} / (\text{H}_2\text{O} + \text{CO}_2 + \text{NaCl}) \text{ in moles}]$, $X_{\text{CO}_2} [= \text{CO}_2 / (\text{H}_2\text{O} + \text{CO}_2 + \text{NaCl}) \text{ in moles}]$, Abbreviations: Tot., total; S., solid; L., liquid; V., vapor, and F, fluid. 3D indicates that the composition was reconstructed from three-dimensional observations of the fluid inclusion (Fig. 7c), whereas 2D indicates that the reconstructed fluid composition was estimated using a representative cross-section of the SR-XCT data of the multiphase-solid fluid inclusion (Fig. 7b)

26.3 wt. % NaCl eq. (Roedder 1984). The eutectic melting temperature for three HI-free primary FIs in Qz is -32.8°C , which is similar to the eutectic melting temperature of the $\text{MgCl}_2\text{-H}_2\text{O}$ system (Table 3) (Davis et al. 1990; Samson and Walker 2000). The homogenization temperatures (T_h) of vapor and liquid in HI-free primary FIs ranged from 136 to 196°C (Fig. 8a, b; Table 3).

Type I and II secondary FIs in Qz show contrasting salinity ranges (Fig. 5a). The T_{mt} values of the type I secondary FIs ranged from -8.7 to -12.4°C , corresponding to a salinity

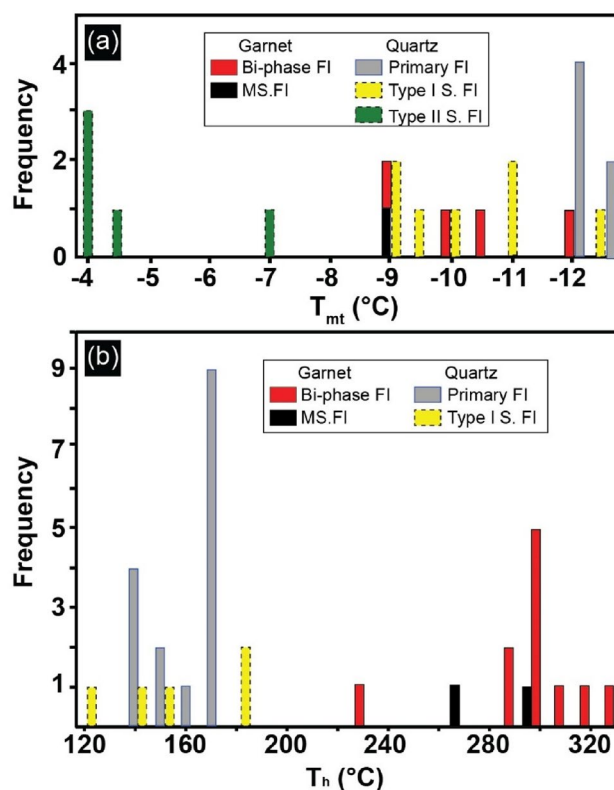


Fig. 8 Frequency histograms of the microthermometric measurements. **a** For ice melting temperatures (T_{mt} ($^\circ\text{C}$)). **b** For homogenization temperatures (T_h ($^\circ\text{C}$)). *FI* fluid inclusion, *MS.FI* multiphase-solid fluid inclusion, *Type I S.FI* Type I secondary fluid inclusion, and *Type II S.FI* Type II secondary fluid inclusion

of 12.5–16.3 wt. % NaCl eq., whereas the T_{mt} values of type II secondary FIs range from -4 to -7.1°C , corresponding to a salinity of 6.4–10.6 wt. % NaCl eq. (Fig. 8a; Table 3). T_h of type I secondary FIs in Qz range from 117 to 181°C . The eutectic melting temperature of 36°C for the type II secondary FI in Qz may contain measurement errors due to its geometry and size. However, this low eutectic melting behavior may be attributed to the solute of divalent cations such as Mg or Fe (Table 3; Borisenko 1977; Davis et al. 1990).

Fluid inclusions in garnet

The T_{mt} and T_h values are determined to be -9.2 to -12.2°C and $231\text{--}327^\circ\text{C}$, respectively, from the bi-phase FIs, and -9°C and $270\text{--}303^\circ\text{C}$, respectively, from the multiphase-solid FIs (Fig. 8a, b; Table 3). The salinity of the bi-phase FIs in Grt is 13–16.1 wt. % NaCl eq., based on the ice melting temperature (Table 3). According to HI observations in the multiphase-solid FIs in Grt, the salinity of these FIs is higher than 26.3 wt. % NaCl eq. (Fig. 7; Fig. S4); in contrast, the salinity of HI-free multiphase-solid FI in Grt is

12.9 wt. % NaCl eq. (Table 3; Fig. 8b; Fig. S4). The eutectic melting temperature of bi-phase FI in Grt is $-37.8\text{ }^{\circ}\text{C}$, which is consistent with that in the $\text{MgCl}_2\text{-KCl-H}_2\text{O}$ fluid system (Table 3; Davis et al. 1990; Dubois and Marignac 1997; Bakker and Baumgartner 2012).

Discussion

Timing of fluid trapping for various types of fluid inclusion in the Khungui eclogite

The primary FIs in Qz and Grt isochores intersect the inferred pressure and temperature (P - T) paths of the Khungui eclogite, between 0.20 and 0.75 GPa and 580–610 $^{\circ}\text{C}$ which is much lower compared to the eclogite facies P - T conditions (Fig. 9a). This suggests that the density could have changed owing to plastic deformation of the host phase

after fluid trapping (Küster and Stöckhert 1997). Therefore, in this study, we discuss the entrapment stage of FIs based on the petrographic description of the FI-hosting minerals.

The mineral inclusions (Omp, Brs, Rt, Qz, and Ep) indicate that the Ca-rich rim of Grt formed at the eclogite facies conditions (Figs. 3a, 4a), with estimated P - T conditions at 2.1–2.2 GPa and 580–610 $^{\circ}\text{C}$ (Bayarbold et al. 2022). The bi-phase FIs occur in both the Ca-poor core and inner parts of the Ca-rich rim of Grt, whereas the multiphase-solid FIs occur only in the outer parts of the Ca-rich rims (Fig. 3e, h). Such distinct spatial distributions of the two types of FIs indicate that bi-phase FIs were trapped in Grt during the prograde stage to the early eclogite-stage of metamorphism, whereas multiphase-solid FIs were trapped during the later stages of eclogite facies conditions (Fig. 9a).

In contrast to the FIs in Grt, it is difficult to constrain the timing of formation of primary FIs in Qz, because Qz is stable over the entire range of P - T conditions estimated for

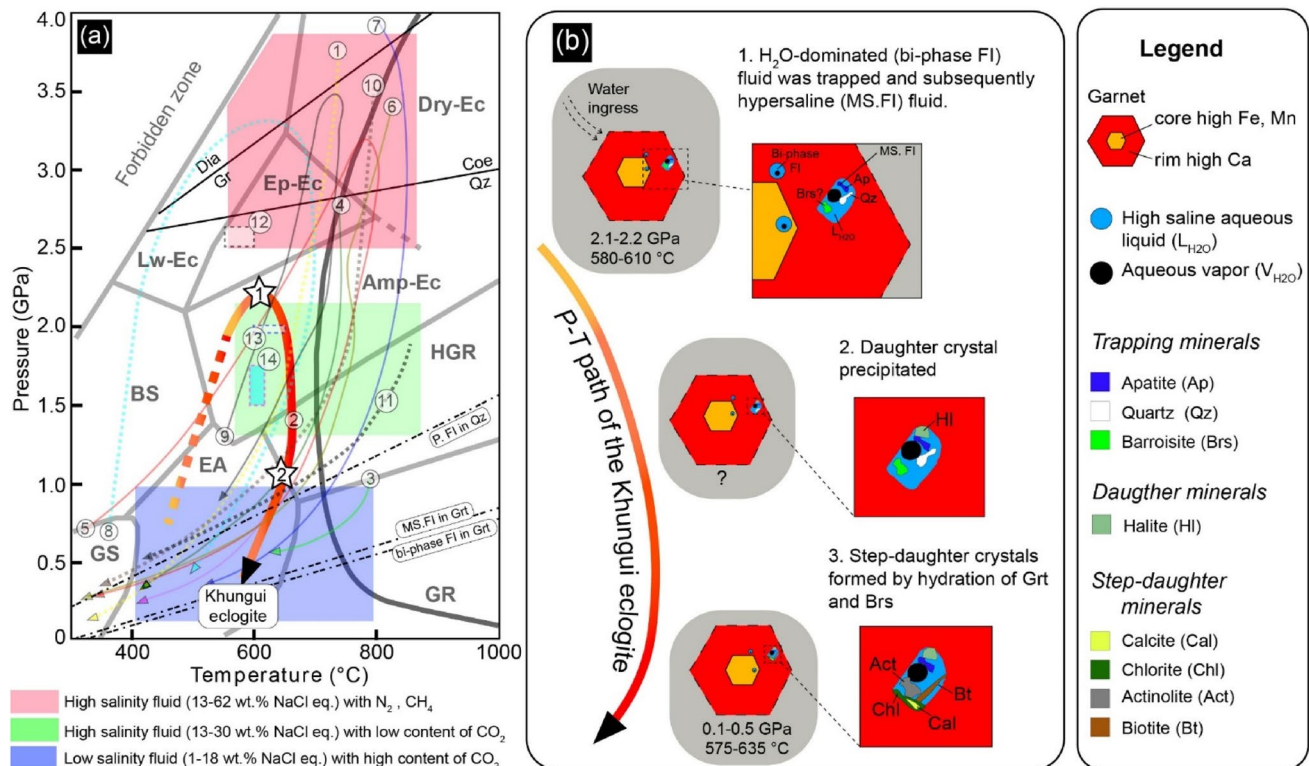


Fig. 9 **a** P - T fluid path for the Khungui eclogite. Previous reports of salinity and some volatiles (N_2 , CH_4 , and CO_2) during the HP-UHP metamorphism in Paleo-subduction zones. References: (1) Fu et al. (2001); (2) Fu et al. (2002); (3) Fu et al. (2003b); (4) Fu et al. (2003a); (5) Zhang et al. (2005); (6) (Ferrando et al. 2005a); (7) Mukherjee and Sachan (2009); (8) Liu et al. (2019); (9) Philippot et al. (1995); (10) Frezzotti et al. (2007); (11) Xiao et al. (2000); (12) Philippot and Selverstone (1991); (13) Selverstone et al. (1992); (14) Svensen et al. (1999, 2001). Dotted lines present isochore calculations of primary fluid inclusions in the studied sample. The black solid line presents a wet solidus of basalt (Kessel et al. 2005). The

star with numbers shows the fluid infiltration conditions of the studied sample. Isochore abbreviations: P.FI in Qz—primary fluid inclusion in quartz; MS.FI in Grt—multiphase-solid fluid inclusion in garnet; bi-phase FI in Grt—bi-phase fluid inclusion in garnet. Diagram of metamorphic facies modified from Tsujimori and Mattinson (2021). **b** Origin of multiphase-solid fluid inclusion in garnets of the Khungui eclogite. Details are described in the text. Metamorphic facies, Dry-Ec Dry eclogite, Ep-Ec Epidote eclogite, Amp-Ec Amphibole eclogite, Lw-Ec, Lawsonite eclogite, BS blueschist, HGR high-pressure granulite, GR Granulite, EA epidote-amphibolite, GS Greenschist

this sample (Fig. 2a). The primary FIs in the Qz matrix has a high salinity (15.7–16.4 wt. % NaCl eq.), which is identical to the salinity of the bi-phase FIs in Grt (13–16.1 wt. % NaCl eq.), except for the additional occurrence of HI in a limited number of FIs in Qz. Therefore, HI-free primary FIs in Qz can be trapped in the same metamorphic stage as bi-phase FIs in Grt (Fig. 9a, b). The limited HI-bearing FIs in Qz could be related to the partial water leakage or water trapped simultaneously with hypersaline fluid, corresponding to multiphase-solid FIs in Grt, as described in a later section.

The observed occurrences and microthermometric characteristics (12.5–16.3 wt. % NaCl eq.) indicate that the type I secondary FIs in the Qz matrix were formed after eclogite stage metamorphism (Fig. 5a; Table 3). Therefore, the first high salinity event (13–16.4 wt. % NaCl eq.) of fluids occurs at greater depths (~70 km) that corresponds to the eclogite facies metamorphism (2.1–2.2 GPa at 580–610 °C), whereas the second relatively high salinity (12.5–16.3 wt. % NaCl eq.) of fluids are found during the exhumation of the Khungui eclogite (Fig. 9a). In contrast of Type I, Type II secondary FIs with micro-veins may represent fluid infiltration into the Khungui eclogites at later stages of exhumation because that fluid system of Type II secondary FIs (Fe, Mg) Cl₂–H₂O in Qz is completely different from the primary FIs (MgCl₂–H₂O) in Qz and FIs in Grt (Table 3). Moreover, the salinity of Type II secondary FIs in Qz is significantly lower than that of Type I secondary FIs in Qz.

Formation of the multiphase-solid fluid inclusions in garnet

The following three scenarios have been hypothesized as the origin of multiphase-solid mineral inclusions or multiphase-solid FIs, in the anhydrous minerals of HP and UHP rocks (Ferrando et al. 2005a).

- (i) Precipitation from supercritical silicate (C–O–H) fluids of crustal or mantle origin (Stöckhert et al. 2001; van Roermund et al. 2002; Dobrzhinetskaya et al. 2003a; Hwang et al. 2003).
- (ii) Crystallization from residual Mg-rich aqueous (salinities up to 68 wt. % NaCl eq.), generated by partial melting (Philippot 1993; Philippot et al. 1995), or crystallization from silicate melts (Hwang et al. 2001)
- (iii) Reaction of multi-component aqueous fluids with host minerals in deep subduction zones (Philippot and Selverstone 1991; Selverstone et al. 1992; Scambelluri et al. 1998; Svensen and Museum 2001).

In this study, the peak *P–T* conditions (2.1–2.2 GPa at 580–610 °C; Bayarbold et al. 2022) were much lower

than the second critical endpoint of the basalt water system (~5.2 GPa at 1050 °C; Kessel et al. 2005) or the wet solidus of the basaltic system (~2 GPa at 710 °C; Kessel et al. 2005) (Fig. 0.9a). In addition, the multiphase-solid FIs in Grt show a variety of mineral assemblages, including Qz, Cal, Qz + Cal, Amp + mica, Ap + Amp + mica, Cal + Amp + mica, Qz + Amp + Cal + HI, and Cal + Amp + mica + Chl + HI, in addition to the fluid phase (Figs. 4, 6, and 7; Fig. S4; Table 1). Such variations cannot be explained by the crystallization of a single-phase supercritical fluid or melt (hypothesized scenarios (i) or (ii)).

Accordingly, we consider that in scenario (iii), the *in-situ* reactions between the coexisting minerals and aqueous fluids most likely formed the mineralogy of the multiphase-solid FIs observed in Grt. However, the variation in mineralogy (Table 1) and high solid-to-fluid volume ratio could not be explained by simple reactions between aqueous fluids and the host Grt. Therefore, we consider the origin of the observed minerals in the inclusions to be either trapped, daughter, or step-daughter mineral phases (i.e., the product of the inclusion fluid and host and/or coexisting mineral reactions; Svensen et al. 1999).

Ap and Qz commonly occur in the matrix and as mineral inclusions in the Grt (Figs. 2b, c, 3; Table 1; Fig. S4). In addition, variable proportions of Ap and Qz exist in the multiphase-solid FIs (Ap of size 3–10 μm; Qz of size 5–20 μm; Fig. 4a; Fig. S4). These occurrences indicate that Ap and Qz are trapped synchronously with fluid (Fig. 9b). However, the possibility that these minerals grew or dissolved in aqueous fluids cannot be excluded.

The HI crystals in the multiphase-solid FIs of Grt are euhedral (Figs. 5a and 6; Fig. S4), suggesting that HI precipitated directly from the trapped fluid; the results were similar to those commonly reported for other HP and UHP metamorphic rocks (Philippot and Selverstone 1991; Selverstone et al. 1992; Svensen et al. 1999; Svensen and Museum 2001; Zhang et al. 2005; Xiao et al. 2006).

The Cal crystals in the multiphase-solid FIs in Grt are mostly anhedral (Fig. 6, Fig. S4). The SR-XCT images show that Chl and Cal are intercalated along the walls of the host Grt (Fig. 7b, c), suggesting that Chl and Cal might have formed simultaneously via the replacement of Grt. However, the Chl + Cal assemblage is not observed in the 2D view of the multiphase-solid FIs (Table 1; Fig. S4); this could be related to the cutting effect or to the reaction product (Chl) being too minuscule to be observed.

Act and Bt occur exclusively in the multiphase-solid FIs in Grt, but do not occur as matrix minerals or fluid-absent mineral inclusions in the analyzed samples (Figs. 2b, 2c, 3; Table 1). Therefore, we consider that these minerals were formed via hydration reactions between fluids and minerals that were simultaneously trapped in Grt.

Some experimental studies have suggested that fluid–mineral interactions might be as effective and fast as high-salinity fluids, compared to low-salinity fluids (Huang et al. 2023). Thus, we conclude that the lack of reaction products or precipitates in the bi-phase FIs in Grt could be attributed to the relatively low salinity (13–16 wt. % NaCl eq.) of these FIs, compared to the hypersaline fluids to produce primary multiphase-solid FIs in Grt as described in later. In contrast to FIs in Grt, the reaction between FIs in Qz and host Qz is more restricted except for silica. Therefore, mineral phases present in HI-bearing FIs in Qz and the multiphase-solid FIs in Grt formed from hypersaline fluid might exhibit notable differences.

Composition of fluids trapped in the Khungui eclogite under HP condition

Based on the optical microscope, SEM, and Raman spectroscopy observations, we determine the variable mineral assemblages in the multiphase FIs of the studied samples (Figs. 4, 6, and 7; Fig. S4; Table 1). Although the liquid and vapor ratios of bi-phase FIs could be accurately estimated optically (e.g., Bakker and Diamond 2006), the estimation of individual volumes of the solid- and fluid-phases in multiphase-solid FIs is not easy.

A comparison of the total 3D phase-volume proportion to that estimated from a specific 2D cross-section reveal the following significant differences in vol. % of the minerals: Cal (3D, 6 vol. %; 2D, 2 vol. %), Bt (3D, 4 vol. %; 2D, 8 vol. %), and HI (3D, 7 vol. %; 2D, 2 vol. %) (Table 4). Based on these comparisons, we use 3D-SR-XCT data to reconstruct the initial fluid composition of the multiphase-solid FIs, as described in the following section.

We reconstructed the composition of the initial trapped fluid in the $\text{SiO}_2\text{--TiO}_2\text{--FeO--MnO--MgO--CaO--Na}_2\text{O--K}_2\text{O--CO}_2\text{--Cl--H}_2\text{O}$ system, based on the volume (cm^3), density (g/cm^3), and composition (wt. %) of the daughter (HI) and step-daughter minerals (Cal, Chl, Act, and Bt) in the multiphase-solid FIs. The compositions of the initial fluids are estimated using the following mass balance equation:

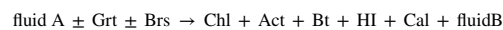
$$m_i^F = \sum_p M_k X_i^k - \sum_r M_k X_i^k \quad (1)$$

Where m_i^F is the molar amount of element i in the reconstructed initial fluid per unit volume of the FI (mol/cm^3 fluid inclusion), M_k is the molar amount of phase k per unit volume of the FI, X_i^k is the molar amount of element i per formula unit of phase k , r , and p in the summation indicate the reactants (Grt and Brs; as explained later) and products (Chl, Act, Bt, Cal, HI, and fluid) of the FI, respectively. M_k is obtained from the observed volume fractions of phase k (F_k) and the molar volume of phase k (V_k), using the formula

$M_k = F_k/V_k$. A mass-balance calculation is conducted on the 3D-SR-XCT data (Fig. 7c; Table 4), and a similar calculation is subsequently performed for the 2D volume estimations for comparison (Table 4).

The compositions of Act and Bt in the exposed multiphase-solid FIs are determined using EPMA (Table 2; Fig. 4), whereas Cal and HI are assumed to be pure CaCO_3 and NaCl, respectively. Chl is assumed to be Fe-dominated based on the semi-quantitative data obtained from the FIB–SEM–EDS analysis (Table 2; Fig. S5).

As discussed in the previous section, it is assumed that the trapped minerals reacted with the fluid, as depicted using the following reaction:



Apart from Grt, which hosts the FIs, we assume Brs to be an additional reactant mineral, since mafic minerals (Chl, Act, and Bt) are formed in the multiphase-solid FI, and Brs is common in the matrix and as inclusions in the Ca-rich rim of Grt (Figs. 3, and 4; Table 1). As the observed liquid in the FI is saturated with HI, the composition of fluid B is assumed to be NaCl saturated at room temperature (i.e., 26.3 wt. % NaCl eq.). The compositions of the Ca-rich rims of Grt and Cl-bearing Brs inclusions (Cl = 1.01 wt. %) are used for mass-balance calculations (Table 2).

The amount of parent minerals (Grt and Brs) that reacted with fluid A are systemically varied in the range of 0–0.20 [$\text{mol}/100 \text{ cm}^3$ FI] (Fig. 10). Increasing the amount of Grt and/or Brs resulted in a decrease in the Si, Al, Fe, Mg, and Ca contents in the initial fluid. The Na, K, Cl, and C contents of the initial fluid are barely affected by the amounts of reactants used. The amount of reacted Grt and/or Brs is limited because of the limited availability of Al, Si, and/or Mg in the bulk FI. As a result, the total amount of dissolved cations is observed to be the lowest (~ 19 molal = $\text{mol/kg H}_2\text{O}$) when Grt and Brs are reacted at ratios of 0.048 and 0.087 ($\text{mol}/100 \text{ cm}^3$ FI), respectively (Fig. 10). Because the solubility of aqueous fluids is limited, we consider this to be the most probable initial fluid composition for the studied multiphase-solid FI.

The estimated elemental concentration of the initial fluid (in molal) are ~ 0 for Si, Ti, Al, and Mn; 2.9 for Fe; 2.1 for Mg; 2.7 for Ca; 10.4 for Na; 0.5 for K; 3.8 for C; and 12.7 for Cl, corresponding to 32.2 wt. % NaCl eq.; $X_{\text{NaCl}} [= \text{NaCl} / (\text{H}_2\text{O} + \text{CO}_2 + \text{NaCl}) \text{ in mol}] = 0.18$ and $X_{\text{CO}_2} [= \text{CO}_2 / (\text{H}_2\text{O} + \text{CO}_2 + \text{NaCl}) \text{ in mol}] = 0.05$ (Table 4). Moreover, $\sim 15\%$ of the H_2O in the initial trapped fluid is consumed in the reaction of Grt and Brs with Chl, Act, and Bt.

The overall results of the reaction are summarized as follows:

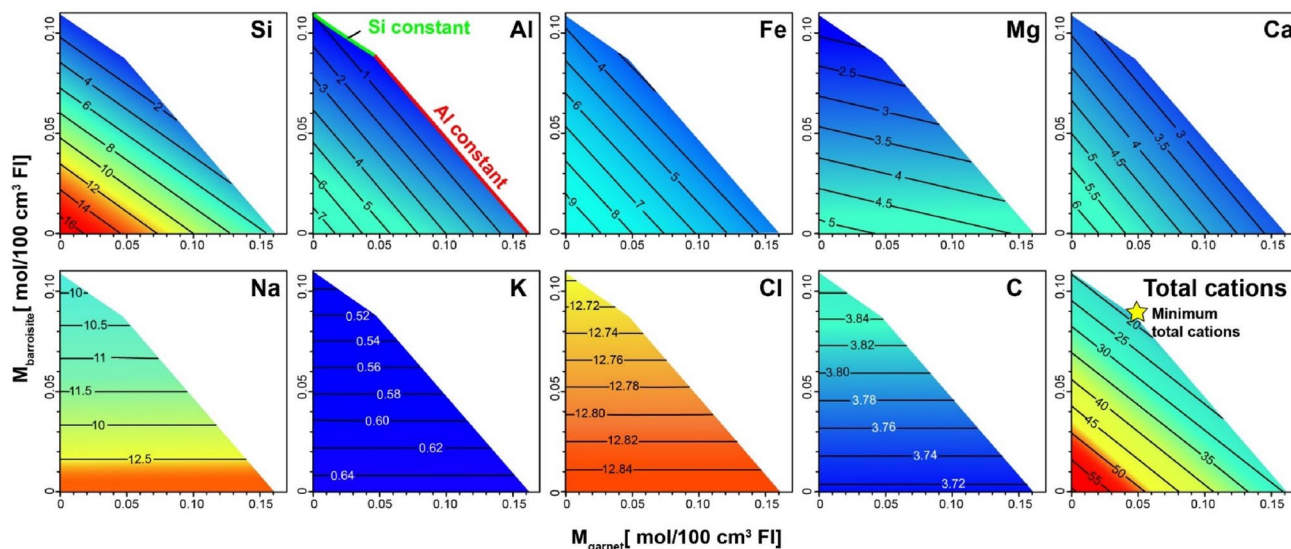
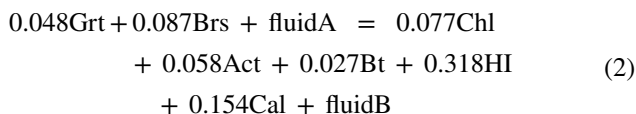


Fig. 10 An example of the reconstructed fluid composition based on 3D data of the multiphase-solid fluid inclusion, as determined by SR-XCT analysis. The variation in solute concentration in the reconstructed fluid is shown with respect to the volumes [mol/100 cm³] of

garnet and barroisite that are involved in the reaction. We have kept the reconstructed fluid composition where the total dissolved component (cations) becomes minimum. For further details, please refer to the text



For comparison, the representative results of the reconstructed initial trapped fluid composition based on 2D observation of the multiphase-solid FI (in molar) are 0 for Si and Al; 0.1 for Ti and Mn; 3.4 for Fe; 2.3 for Mg; 0.7 for Ca; 3.1 for Na; 1.1 for K; 1.5 for C; and 7.0 for Cl, corresponding to 22.8 wt. % NaCl eq.; $X_{\text{NaCl}} = 0.11$ and $X_{\text{CO}_2} = 0.02$ (Table 4). The Ti, Fe, Mn, Mg, and K concentrations in the 2D reconstructed initial fluid composition are estimated to be higher than those in the 3D reconstructed fluid composition; in contrast, the Ca, Na, C, and Cl concentrations are lower in the 2D reconstruction. In addition, not all minerals are fully recognized by 2D analysis (Table 1). This implies that the fluid compositions reconstructed using 2D images have large uncertainties.

The reconstructed fluid composition of the multiphase-solid FIs suggests that the initially trapped fluid at the eclogite stage of the Khungui eclogite was hypersaline (~32.2 wt. % NaCl eq.) and consisted of fluids with variable solute components (Ca, Na, K, Mg, Fe, C, and Cl). In contrast, the bi-phase FIs indicate a relatively high salinity (13–16.1 wt. % NaCl eq.) H₂O-dominated fluid with solutes (Mg and K) is identified based on

microthermometry data (Table 3; Davis et al. 1990; Dubois and Marignac 1997; Bakker and Baumgartner 2012). This suggests that two types of fluids with different characteristics existed during the earlier and later stages of eclogite facies metamorphism.

Possible source of fluid origin

The fluid origin of HP–UHP metamorphism has been explained by internal or external fluid sources based on oxygen isotopes, the composition of FI, and their FI host minerals (Ferrando et al. 2005b, a, 2020; Zhang et al. 2008; Frezzotti and Ferrando 2015). The internal fluid was attributed to the decomposition of hydrous minerals. In contrast, external fluids were more closely related to the dehydration of metasedimentary rocks or the serpentinized mantle in the subduction slab. Some studies have suggested that both fluid origins can coexist at the same metamorphic stage (Spandler et al. 2011).

The bi-phase H₂O-dominated FI (up to 16 wt. % NaCl eq.) indicates ubiquitous occurrence of a highly saline H₂O-dominated fluid at the prograde to eclogite facies stages in the Khungui eclogite. Although the origin of a highly saline fluid under the eclogite facies is unclear, the potential materials for high Cl content with H₂O, that is, Cl-rich hydrous minerals have not been clarified from the prograde stages of the Khungui eclogite (Figs. 2a, 3, 4; Table 1). This suggests the

influence of the infiltration of the highly saline H₂O-dominated external fluid at the prograde to the earlier eclogite facies stage. In contrast, at the later eclogite facies stage, the presence of hypersaline fluids is recorded as multiphase-solid FIs. One mechanism for the production of hypersaline fluids is the formation of hydrous minerals. If H₂O in the above mentioned fluid is consumed for the growth of hydrous minerals (i.e., Brs) in a near-closed system, the solute concentration in the fluid increases, to produce a hypersaline fluid (Markl and Bucher 1998). The increase in Cl content at the rim of the Brs inclusions, the rim of Ap in the matrix, and CO₂ phase (Cal) detected from only multiphase-solid FIs are similarly compatible with such an increase in the solute content in the later eclogite facies (Fig. 3c, Fig. S2).

Variable sizes of the multiphase-solid FI have been commonly reported in the peak mineral assemblages of UHP metamorphic rocks (Fu et al. 2001; Ferrando et al. 2005a, b; Frezzotti et al. 2007; Zhang et al. 2008; Jin et al. 2023) (Fig. 9a). The mineral phases in multiphase-solid FIs consist mainly of hydrous (e.g., Bt, Chl, Amp, and Ep), anhydrous (e.g., Qz, zircon, and pyroxene), and carbonate minerals (e.g., Cal, dolomite, and magnesite), and rarely include sulfates (gypsum), phosphates (Ap and monazite), and oxides (Rt). Mineral observations (Act, Bt, Chl, Cal, HI, Qz, and Ap) of the multiphase-solid FI in Grt from the Khungui eclogite suggest similar aspects to the characteristics of multiphase-solid FIs in UHP metamorphic rocks. However, these multiphase-solid FIs in the UHP metamorphic rocks originated completely different mechanisms. The origin of multiphase-solid FIs in UHP metamorphic rocks was related to melting or supercritical fluids (Frezzotti and Ferrando 2015) in deep subduction zones. Furthermore, in a few cases, the multiphase-solid FIs have been recorded from HP metamorphic rocks such as the HP vein (2.6 GPa, 550 °C) in Monviso (Philippot and Selverstone 1991), eclogitic segregation (2.0 GPa, 625 °C) in the Tauren Window (Selverstone et al. 1992), and eclogite (1.5–1.7 GPa, 600 °C) in the Western Gneiss Region (Svensen and Museum 2001). The *P–T* conditions of the eclogite facies stage of these HP metamorphic rocks are close to the Khungui eclogite (2.1–2.2 GPa, 580–610 °C). Therefore, multiphase-solid FIs in HP metamorphic rocks may have been formed by the mechanism proposed in this study.

The high salinity in the fluid from the Khungui eclogite, evident from the bi-phase aqueous inclusions, is comparable to that reported for HP metamorphic rocks, but not UHP rock. The salinity of the decompression fluid in the Khungui eclogite remains high (up to 15 wt. % NaCl eq.) (Fig. 9a), similar to the characteristics reported for the decompression stage fluids of the Makbal UHP complex in the Kyrgyz Tianshan area, CAO (Orozbaev et al. 2015; Yoshida et al. 2016).

Conclusions

- (1) Garnets and quartz in the Khungui eclogite of the Zavkhan Terrane, western Mongolia, contain various types of fluid inclusions and multiphase-solid fluid inclusions trapped at the eclogite facies conditions and decompression stages. Both bi-phase aqueous inclusions and multiphase-solid fluid inclusions, including halite, are recognized as primary inclusions in garnet and quartz, exhibiting a high salinity of 13–16.4 wt. % NaCl eq. and > 26.4 wt. % NaCl eq., respectively. Relatively high salinity aqueous fluids (< 16 wt. % NaCl eq.) in quartz were also present during the subsequent decompression.
- (2) Primary multiphase-solid fluid inclusions in garnet contain a variety of mineral assemblages, primarily calcite, amphibole, and mica, as well as rare halite, quartz, chlorite, and apatite.
- (3) Precise mass balance analyses were conducted based on the estimates of the volumes of all phases in the multiphase-solid fluid inclusions in garnet, using synchrotron X-ray CT data. About ~ 15% of H₂O was consumed during the reactions between the trapped fluids and minerals.
- (4) Based on the fluid inclusion observations, the following deep fluid history was suggested for the Khungui eclogite: (i) H₂O-dominated fluids with high salinity (13–16.4 wt.% NaCl eq.) and certain solute compounds (Na, Mg, and K) infiltrated the rocks during prograde to the earlier eclogite facies stages, and (ii) the desiccation of aqueous fluids took place at the later stage of the eclogite facies metamorphism due to the growth of hydrous minerals and hypersaline fluids (~ 32.2 wt. % NaCl eq.) with variable solute components (Fe, Mg, Ca, Na, C, and Cl) were produced at later stage of the eclogite facies metamorphism, probably due to the growth of hydrous minerals, and (iii) during exhumation, *in-situ* fluids–mineral reaction occurred in the multiphase-solid fluid inclusions involving the host minerals, as well as other trapped minerals, such that various mineral assemblages in the multiphase-solid fluid inclusions were dependent on the initial trapped minerals in such inclusions.

Supplementary Information The online version contains supplementary material available at <https://doi.org/10.1007/s00410-023-02055-3>.

Acknowledgements This work is part of the first author's Ph.D. thesis submitted to the Graduate School of Environmental Studies, Tohoku University. We would like to express our gratitude to O. Gerel, B. Munkhtsengel, B. Batkhisig, and A. Chimedtsereen for introducing us to this field of study and providing advice. Furthermore, we are grateful to Kazuki Yoshida and Luis Salalá for assisting us in analyzing the data obtained from synchrotron X-ray CT and creating a 3D model of the

fluid inclusions. We also thank Daniela Rubatto, Simona Ferrando, and one anonymous reviewer for their insightful suggestions that helped us to improve the paper. This work is supported financially by JSPS KAKENHI grants JP17H02981, JP22H04932, and JP22H05295 [to A.O.]; JP25000009, and JST/JICA SATREPS JPMJSA1703 [to N.T.]; JP22H01329, and JP22H05296 [to M.U.]; JP19K14825 [to K.Y.]; and Grant-in-Aid for Transformative Research Areas (A) JP22H05109 [to Y.N. and M.K.].

Author contributions AO and NT designed the study; MB, AK, GA, OD, and MU performed the study; MB, GA, AK, KY, YN, and MK analyzed the data; and MB, AO, MU, and KY wrote the paper. The authors declare that they have no known competing financial interests or personal relationships that could have influenced the work reported in this study.

Data availability The datasets generated and analyzed during the current study are available from the corresponding author on reasonable request.

Declarations

Conflict of interest The authors declare no competing interests.

Open Access This article is licensed under a Creative Commons Attribution 4.0 International License, which permits use, sharing, adaptation, distribution and reproduction in any medium or format, as long as you give appropriate credit to the original author(s) and the source, provide a link to the Creative Commons licence, and indicate if changes were made. The images or other third party material in this article are included in the article's Creative Commons licence, unless indicated otherwise in a credit line to the material. If material is not included in the article's Creative Commons licence and your intended use is not permitted by statutory regulation or exceeds the permitted use, you will need to obtain permission directly from the copyright holder. To view a copy of this licence, visit <http://creativecommons.org/licenses/by/4.0/>.

References

- Badarch G, Dickson Cunningham W, Windley BF (2002) A new terrane subdivision for Mongolia: implications for the Phanerozoic crustal growth of Central Asia. *J Asian Earth Sci* 21:87–110. [https://doi.org/10.1016/S1367-9120\(02\)00017-2](https://doi.org/10.1016/S1367-9120(02)00017-2)
- Bakker RJ, Baumgartner M (2012) Unexpected phase assemblages in inclusions with ternary H₂O-salt fluids at low temperatures. *Cent Eur J Geosci* 4:225–237. <https://doi.org/10.2478/s13533-011-0047-x>
- Bakker RJ, Diamond LW (2006) Estimation of volume fractions of liquid and vapor phases in fluid inclusions, and definition of inclusion shapes. *Am Mineral* 91:635–657. <https://doi.org/10.2138/am.2006.1845>
- Bayarbold M, Okamoto A, Dandar O et al (2022) Continental arc-derived eclogite in the Zavkhan terrane, western Mongolia: implications for the suture zone in the northern part of the Central Asian orogenic belt. *J Asian Earth Sci*. <https://doi.org/10.1016/j.jseaes.2022.105150>
- Bodnar RJ (1993) Revised equation and table for determining the freezing point depression of H₂O-NaCl solutions. *Geochim Cosmochim Acta* 57:683–684. [https://doi.org/10.1016/0016-7037\(93\)90378-A](https://doi.org/10.1016/0016-7037(93)90378-A)
- Bodnar RJ (2003) Chapter 4: Introduction to aqueous-electrolyte fluid systems
- Bold U, Crowley JL, Smith EF et al (2016) Neoproterozoic to early Paleozoic tectonic evolution of the Zavkhan terrane of Mongolia: Implications for continental growth in the Central Asian orogenic belt. *Lithosphere* 8:729–750. <https://doi.org/10.1130/L549.1>
- Borisenko AS (1977) Study of the salt composition of solutions in gas-liquid inclusions in minerals by the cryometric method. *Sov Geol Geophys* 18:11–19
- Connolly JAD, Galvez ME (2018) Electrolytic fluid speciation by Gibbs energy minimization and implications for subduction zone mass transfer. *Earth Planet Sci Lett* 501:90–102. <https://doi.org/10.1016/j.epsl.2018.08.024>
- Davis DW, Lowenstein TK, Spencer RJ, (1990) Melting behavior of fluid inclusions in laboratory-grown halite crystals in the systems NaCl-H₂O, NaCl-KCl-H₂O, NaCl-MgCl₂-H₂O, and NaCl-CaCl₂-H₂O*. *Geochim Cosmochim Acta* 54:591–601. <https://reader.elsevier.com/>
- De Corte K, Cartigny P, Shatsky VS et al (1998) Evidence of fluid inclusions in metamorphic microdiamonds from the Kokchetav massif, northern Kazakhstan. *Geochim Cosmochim Acta* 62:3765–3773. [https://doi.org/10.1016/S0016-7037\(98\)00266-X](https://doi.org/10.1016/S0016-7037(98)00266-X)
- Dobrzhinetskaya LF, Green HW, Bozhilov KN, Mitchell TE (2003a) Crystallization environment of Kazakhstan microdiamond: evidence from nanometric inclusions and mineral associations. *J Metamorph Geol* 21:425–437
- Dobrzhinetskaya LF, Green HW, Weschler M et al (2003b) Focused ion beam technique and transmission electron microscope studies of microdiamonds from the Saxonian Erzgebirge, Germany. *Earth Planet Sci Lett* 210:399–410. [https://doi.org/10.1016/S0012-821X\(03\)00170-5](https://doi.org/10.1016/S0012-821X(03)00170-5)
- Dobrzhinetskaya LF, Wirth R, Green HW, (2005) Direct observation and analysis of a trapped COH fluid growth medium in metamorphic diamond. *Terra Nov* <https://doi.org/10.1111/j.1365-3121.2005.00635.x>
- Dubois M, Marignac C (1997) The H₂O-NaCl-MgCl₂ ternary phase diagram with special application to fluid inclusion studies. *Econ Geol* 92:114–119. <https://doi.org/10.2113/gsecongeo.92.1.114>
- Ferrando S, Frezzotti ML, Dallai L, Compagnoni R (2005a) Multiphase solid inclusions in UHP rocks (Su-Lu, China): remnants of supercritical silicate-rich aqueous fluids released during continental subduction. *Chem Geol* 223:68–81. <https://doi.org/10.1016/j.chemgeo.2005.01.029>
- Ferrando S, Frezzotti ML, Dallai L, Compagnoni R (2005b) Fluid-Rock Interaction in UHP Phengite-Kyanite-Epidote Eclogite from the Sulu Orogen, Eastern China. *Int Geol Rev* 47:750–774. <https://doi.org/10.2747/0020-6814.47.7.750>
- Ferrando S, Frezzotti ML, Petrelli M, Compagnoni R (2009) Metasomatism of continental crust during subduction: The UHP whiteschists from the Southern Dora-Maira Massif (Italian Western Alps). *J Metamorph Geol* 27:739–756. <https://doi.org/10.1111/j.1525-1314.2009.00837.x>
- Ferrando S, Groppo C, Frezzotti ML et al (2017) Dissolving dolomite in a stable UHP mineral assemblage: Evidence from Cal-Dol marbles of the Dora-Maira Massif (Italian Western Alps). *Am Mineral* 102:42–60. <https://doi.org/10.2138/am-2017-5761>
- Ferrando S, Petrelli M, Frezzotti ML (2020) Trace-element Behavior in UHP fluid inclusions: indicator of the petrological and geochemical evolution of the Slab-released fluids. Abstract on line. <https://doi.org/10.4647/gold2020.711>
- Frezzotti ML, Ferrando S (2015) The chemical behavior of fluids released during deep subduction based on fluid inclusions. *Am Mineral* 100:352–377. <https://doi.org/10.2138/am-2015-4933>
- Frezzotti ML, Ferrando S, Dallai L, Compagnoni R (2007) Intermediate alkali - Aluminosilicate aqueous Solutions released by deeply subducted continental crust: fluid evolution in UHP OH-rich topaz - kyanite quartzites from Donghai (Sulu, China). *J Petrol* 48:1219–1241. <https://doi.org/10.1093/petrology/egm015>

- Frezzotti ML, Selverstone J, Sharp ZD, Compagnoni R (2011) Carbonate dissolution during subduction revealed by diamond-bearing rocks from the Alps. *Nat Geosci* 4:703–706. <https://doi.org/10.1038/ngeo1246>
- Fu B, Touret JLR, Zheng YF (2001) Fluid inclusions in coesite-bearing eclogites and jadeite quartzite at Shuanghe, Dabie Shan (China). *J Metamorph Geol* 19:531–547. <https://doi.org/10.1046/j.0263-4929.2001.00327.x>
- Fu B, Zheng YF, Touret JLR (2002) Petrological, isotopic and fluid inclusion studies of eclogites from Sujiahe, NW Dabie Shan (China). *Chem Geol* 187:107–128. [https://doi.org/10.1016/S0009-2541\(02\)00014-1](https://doi.org/10.1016/S0009-2541(02)00014-1)
- Fu B, Touret JLR, Zheng YF (2003a) Remnants of premetamorphic fluid and oxygen isotopic signatures in eclogites and garnet clinopyroxenite from the Dabie-Sulu terranes, eastern China. *J Metamorph Geol* 21:561–578. <https://doi.org/10.1046/j.1525-1314.2003.00464.x>
- Fu B, Touret JLR, Zheng YF, Jahn BM (2003b) Fluid inclusions in granulites, granulitized eclogites and garnet clinopyroxenites from the Dabie - Sulu terranes, eastern China. *Lithos* 70:293–319. [https://doi.org/10.1016/S0024-4937\(03\)00103-8](https://doi.org/10.1016/S0024-4937(03)00103-8)
- Galvez ME, Connolly JAD, Manning CE (2016) Implications for metal and volatile cycles from the pH of subduction zone fluids. *Nature* 539:420–424. <https://doi.org/10.1038/nature20103>
- Gao J, Klemd R (2001) Primary fluids entrapped at blueschist to eclogite transition: Evidence from the Tianshan meta-subduction complex in Northwestern China. *Contrib to Mineral Petrol* 142:1–14. <https://doi.org/10.1007/s004100100275>
- Giarmita MJ, Sorensen SS (1994) Primary fluids in low-temperature eclogites: evidence from two subduction complexes (Dominican Republic, and California, USA). *Contrib to Mineral Petrol* 117:279–292. <https://doi.org/10.1007/BF00310869>
- Huang F, Sverjensky DA (2019) Extended deep earth water model for predicting major element mantle metasomatism. *Geochim Cosmochim Acta* 254:192–230. <https://doi.org/10.1016/j.gca.2019.03.027>
- Huang R, Shang X, Zhao Y et al (2023) Effect of fluid salinity on reaction rate and Molecular hydrogen (H₂) formation during Peridotite Serpentinization at 300 °C. *J Geophys Res Solid Earth* 128:1–17. <https://doi.org/10.1029/2022JB025218>
- Hwang SL, Shen P, Chu HT et al (2001) Genesis of microdiamonds from melt and associated multiphase inclusions in garnet ultrahigh-pressure gneiss from Erzgebirge, Germany. *Earth Planet Sci Lett* 188:9–15. [https://doi.org/10.1016/S0012-821X\(01\)00314-4](https://doi.org/10.1016/S0012-821X(01)00314-4)
- Hwang SL, Shen P, Yui TF, Chu HT (2003) Metal-sulfur-COH-silicate fluid mediated diamond nucleation in Kokchetav ultrahigh-pressure gneiss. *Eur J Mineral* 15:503–511. <https://doi.org/10.1127/0935-1221/2003/0015-0503>
- Hwang SL, Chu HT, Yui TF et al (2006) Nanometer-size P/K-rich silica glass (former melt) inclusions in microdiamond from the gneisses of Kokchetav and Erzgebirge massifs: diversified characteristics of the formation media of metamorphic microdiamond in UHP rocks due to host-rock buffering. *Earth Planet Sci Lett* 243:94–106. <https://doi.org/10.1016/j.epsl.2005.12.015>
- Jin D, Xiao Y, Tan D et al (2023) Supercritical fluid in deep subduction zones as revealed by multiphase fluid inclusions in an ultrahigh-pressure metamorphic vein. *Proc Natl Acad Sci* 120:1–9. <https://doi.org/10.1073/pnas>
- Kawamoto T, Hertwig A, Schertl HP, Maresch WV (2018) Fluid inclusions in jadeite and jadeite-rich rock from serpentinite mélanges in northern Hispaniola: Trapped ambient fluids in a cold subduction channel. *Lithos* 308:227–241. <https://doi.org/10.1016/j.lithos.2018.02.024>
- Kessel R, Ulmer P, Pettke T et al (2005) The water-basalt system at 4 to 6 GPa: Phase relations and second critical endpoint in a K-free eclogite at 700 to 1400 °C. *Earth Planet Sci Lett* 237:873–892. <https://doi.org/10.1016/j.epsl.2005.06.018>
- Korsakov AV, Hermann J (2006) Silicate and carbonate melt inclusions associated with diamonds in deeply subducted carbonate rocks. *Earth Planet Sci Lett* 241:104–118. <https://doi.org/10.1016/j.epsl.2005.10.037>
- Korsakov AV, Dieing T, Golovin AV, Toporski J (2011) Raman imaging of fluid inclusions in garnet from UHPM rocks (Kokchetav massif, Northern Kazakhstan). *Spectrochim Acta - Part A Mol Biomol Spectrosc* 80:88–95. <https://doi.org/10.1016/j.saa.2011.01.035>
- Korsakov AV. (2018) Application of raman imaging in UHPM research. Springer International Publishing
- Kovach V, Kozakov I, Kröner A et al (2021) Early neoproterozoic crustal growth and microcontinent formation of the north-central Central Asian Orogenic Belt: New geological, geochronological, and Nd–Hf isotopic data on the Mélange Zone within the Zavkhan terrane, western Mongolia. *Gondwana Res* 91:254–276. <https://doi.org/10.1016/j.gr.2020.12.022>
- Kozakov IK, Kovach VP, Salnikova EB et al (2021) Formation of the neoproterozoic continental crust in the structures of the Central segment of the Central Asian fold belt. *Petrology* 29:195–220. <https://doi.org/10.1134/S0869591121020053>
- Küster M, Stöckhert B (1997) Density changes of fluid inclusions in high-pressure low-temperature metamorphic rocks from crete: a thermobarometric approach based on the creep strength of the host minerals. *Lithos* 41:151–167. [https://doi.org/10.1016/s0024-4937\(97\)82010-5](https://doi.org/10.1016/s0024-4937(97)82010-5)
- Lanari P, Vidal O, De AV et al (2014) Computers and geosciences XMapTools : A MATLAB © -based program for electron microprobe X-ray image processing and geothermobarometry. *Comput Geosci* 62:227–240. <https://doi.org/10.1016/j.cageo.2013.08.010>
- Li X, Xiaoming S, Wei Z et al (2006) Fluid inclusions in quartz veins from HP-UHP metamorphic rocks, chinese continental scientific drilling (CCSD) project. *Int Geol Rev* 48:639–649. <https://doi.org/10.2747/0020-6814.48.7.639>
- Li H, Zhang L, Christy AG (2011) The correlation between raman spectra and the mineral composition of muscovite and phengite. Elsevier Inc.
- Liu H, Xiao Y, van den Kerkhof A et al (2019) Metamorphism and fluid evolution of the Sumdo eclogite, Tibet: constraints from mineral chemistry, fluid inclusions and oxygen isotopes. *J Asian Earth Sci* 172:292–307. <https://doi.org/10.1016/j.jseae.2018.09.013>
- Maffei A, Ferrando S, Connolly JAD et al (2021) Thermodynamic analysis of HP-UHP fluid inclusions: the solute load and chemistry of metamorphic fluids. *Geochim Cosmochim Acta* 315:207–229. <https://doi.org/10.1016/j.gca.2021.08.044>
- Markl G, Bucher K (1998) Composition of fluids in the lower crust inferred from metamorphic salt in lower crustal rocks. *Nature* 391:781–783. <https://doi.org/10.1038/35836>
- Mikhno AO, Schmidt U, Korsakov AV (2014) Origin of K-cymrite and kokchetavite in the polyphase mineral inclusions from Kokchetav UHP calc-silicate rocks: evidence from confocal Raman imaging. *Eur J Mineral* 25:807–816. <https://doi.org/10.1127/0935-1221/2013/0025-2321>
- Mukherjee BK, Sachan HK (2009) Fluids in coesite-bearing rocks of the Tso Moriri complex, NW Himalaya: evidence for entrapment during peak metamorphism and subsequent uplift. *Geol Mag* 146:876–889. <https://doi.org/10.1017/S0016756809990069>
- Niwa Y, Takeichi Y, Watanabe T, Kimura M (2019) Development of spectromicroscopes for multiscale observation of heterogeneity in materials at photon factory, IMSS, KEK. *AIP Conf Proc* 2054:10–15. <https://doi.org/10.1063/1.5084621>
- Okamoto A, Musya M, Hashimoto Y, Tsuchiya N (2014) Distribution of CO₂ fluids in the Shimanto belt on Muroto Peninsula,

- SW Japan: possible injection of magmatic CO₂ into the accretionary prism. *Earth, Planets Sp* 66:1–9. <https://doi.org/10.1186/1880-5981-66-33>
- Okamoto A, Oyanagi R, Yoshida K et al (2021) Rupture of wet mantle wedge by self-promoting carbonation. *Commun Earth Environ* 2:1–10. <https://doi.org/10.1038/s43247-021-00224-5>
- Orozbaev R, Hirajima T, Bakirov A et al (2015) Trace element characteristics of clinozoisite pseudomorphs after lawsonite in talc-garnet-chloritoid schists from the Makbal UHP Complex, northern Kyrgyz Tian-Shan. *Lithos* 226:98–115. <https://doi.org/10.1016/j.lithos.2014.10.008>
- Perchuk AL, Burchard M, Maresch WV, Schertl HP (2008) Melting of hydrous and carbonate mineral inclusions in garnet host during ultrahigh pressure experiments. *Lithos* 103:25–45. <https://doi.org/10.1016/j.lithos.2007.09.008>
- Perchuk AL, Burchard M, Maresch W V., Schertl H-P (2005) Fluid-mediated modification of garnet interiors under ultrahigh-pressure conditions. *Terra Nov* 17:545–553. <https://onlinelibrary.wiley.com/doi/epdf/https://doi.org/10.1111/j.1365-3121.2005.00647.x>
- Philippot P (1993) Fluid-melt-rock interaction in mafic eclogites and coesite-bearing metasediments: constraints on volatile recycling during subduction. *Chem Geol* 108:93–112. [https://doi.org/10.1016/0009-2541\(93\)90319-E](https://doi.org/10.1016/0009-2541(93)90319-E)
- Philippot P, Selverstone J (1991) Trace-element-rich brines in eclogitic veins: implications for fluid composition and transport during subduction. *Contrib to Mineral Petrol* 106:417–430. <https://doi.org/10.1007/BF00321985>
- Philippot P, Chevallier P, Chopin C, Dubessy J (1995) Fluid composition and evolution in coesite-bearing rocks (Dora-Maira massif, Western Alps): implications for element recycling during subduction. *Contrib to Mineral Petrol* 121:29–44. <https://doi.org/10.1007/s004100050088>
- Ravna EK (2000) The garnet-clinopyroxene Fe²⁺ – Mg geothermometer : an updated calibration. *J Metamorph Geol* 18:211–219
- Ravna EJK, Terry MP (2004) Geothermobarometry of UHP and HP eclogites and schists - An evaluation of equilibria among garnet-clinopyroxene-kyanite-phengite-coesite/quartz. *J Metamorph Geol* 22:579–592. <https://doi.org/10.1111/j.1525-1314.2004.00534.x>
- Roedder E (1984) Volume:12: fluid inclusions. “Reviews in mineralogy”, 12
- Safonova I, Kotlyarov A, Krivonogov S, Xiao W (2017) Intra-oceanic arcs of the Paleo-Asian Ocean. *Gondwana Res* 50:167–194. <https://doi.org/10.1016/j.gr.2017.04.005>
- Samson IM, Walker RT (2000) NaCl–CaCl₂–H₂O And implications FOR low-Temperature phase behavior in aqueous fluid inclusions. 38:35–43
- Scambelluri M, Philippot P (2001) Deep fluids in subduction zones. *Lithos* 55:213–227. [https://doi.org/10.1016/S0024-4937\(00\)00046-3](https://doi.org/10.1016/S0024-4937(00)00046-3)
- Scambelluri M, Pennacchioni G, Philippot P (1998) Salt-rich aqueous fluids formed during eclogitization of metabasites in the alpine continental crust (Austroalpine Mt. Emilius unit, Italian western Alps). *Lithos* 43:151–167. [https://doi.org/10.1016/S0024-4937\(98\)00011-5](https://doi.org/10.1016/S0024-4937(98)00011-5)
- Selverstone J, Franz G, Thomas S, Getty S (1992) Fluid variability in 2 GPa eclogites as an indicator of fluid behavior during subduction. *Contrib to Mineral Petrol* 112:341–357. <https://doi.org/10.1007/BF00310465>
- Şengör AMC, Natal’In BA, Burtman VS (1993) Evolution of the Altaid tectonic collage and Palaeozoic crustal growth in Eurasia. *Nature* 364:299–307. <https://doi.org/10.1038/364299a0>
- Shen K, Zhang Z, Van Den Kerkhof AM et al (2003) Unusual high-density and saline aqueous inclusions in ultrahigh pressure metamorphic rocks from Sulu terrane in eastern China. *Chinese Sci Bull* 48:2018–2023. <https://doi.org/10.1360/02wd0536>
- Skuzovatov S, Shatsky V, Wang KL (2019) Continental subduction during arc-microcontinent collision in the southern Siberian craton: constraints on protoliths and metamorphic evolution of the North Muya complex eclogites (Eastern Siberia). *Lithos* 342–343:76–96. <https://doi.org/10.1016/j.lithos.2019.05.022>
- Spandler C, Pettker T, Rubatto D (2011) Internal and external fluid sources for eclogite-facies veins in the Monviso Meta-ophiolite, Western Alps: implications for fluid flow in subduction zones. *J Petrol* 52:1207–1236. <https://doi.org/10.1093/petrology/egr025>
- Stepanov AS, Hermann J, Korsakov AV, Rubatto D (2014) Geochemistry of ultrahigh-pressure anatexis: fractionation of elements in the Kokchetav gneisses during melting at diamond-facies conditions. *Contrib to Mineral Petrol* 167:1–25. <https://doi.org/10.1007/s00410-014-1002-x>
- Stepanov AS, Hermann J, Rubatto D et al (2016) Melting history of an ultrahigh-pressure paragneiss revealed by multiphase solid inclusions in garnet, Kokchetav massif, Kazakhstan. *J Petrol* 57:1531–1554. <https://doi.org/10.1093/petrology/egw049>
- Stöckhert B, Duyster J, Trepmann C (2001) Microdiamond daughter crystals precipitated from supercritical CO₂ + silicate fluids included in garnet, Erzgebirge, Germany. *Geology* 29:391–394
- Stöckhert B, Trepmann CA, Massonne HJ (2009) Decrepitated UHP fluid inclusions: About diverse phase assemblages and extreme decompression rates (Erzgebirge, Germany). *J Metamorph Geol* 27:673–684. <https://doi.org/10.1111/j.1525-1314.2009.00835.x>
- Svensen H, Jamtveit B, Yardley B et al (1999) Lead and bromine enrichment in eclogite-facies fluids: Extreme fractionation during lower-crustal hydration. *Geology* 27:467–470. [https://doi.org/10.1130/0091-7613\(1999\)027%3c0467:LABEIE%3e2.3.CO;2](https://doi.org/10.1130/0091-7613(1999)027%3c0467:LABEIE%3e2.3.CO;2)
- Svensen H, Museum M (2001) Halogen contents of eclogite facies fluid inclusions and minerals : Caledonides, western Norway
- Tomkins HS, Powell R, Ellis DJ (2007) The pressure dependence of the zirconium-in-rutile thermometer. *J Metamorph Geol* 25:703–713. <https://doi.org/10.1111/j.1525-1314.2007.00724.x>
- Tsujimori T, Mattinson C (2021) Eclogites in different tectonic settings. *Encycl Geol*. <https://doi.org/10.1016/b978-0-08-102908-4.00104-1>
- van Roermund HLM, Carswell DA, Drury MR, Heijboer TC (2002) Microdiamonds in a megacrystic garnet websterite pod from Bardane on the island of Fjorfto, western Norway: Evidence for diamond formation in mantle rocks during deep continental subduction. *Geology* 30:959–962. [https://doi.org/10.1130/0091-7613\(2002\)030%3c0959:MIAMGW%3e2.0.CO;2](https://doi.org/10.1130/0091-7613(2002)030%3c0959:MIAMGW%3e2.0.CO;2)
- Whitney DL, Evans BW (2010) Abbreviations for names of rock-forming minerals. *Am Mineral* 95:185–187. <https://doi.org/10.2138/am.2010.3371>
- Xiao Y, Hoefs J, Van Den Kerkhof AM et al (2000) Fluid history of UHP metamorphism in Dabie Shan, China: A fluid inclusion and oxygen isotope study on the coesite-bearing eclogite from Bixiling. *Contrib to Mineral Petrol* 139:1–16. <https://doi.org/10.1007/s004100050570>
- Xiao Y, Hoefs J, Van Den Kerkhof AM et al (2002) Fluid evolution during HP and UHP metamorphism in Dabie Shan, China: constraints from mineral chemistry, fluid inclusions and stable isotopes. *J Petrol* 43:1505–1527. <https://doi.org/10.1093/petrology/43.8.1505>
- Xiao Y, Zhang Z, Hoefs J, van den Kerkhof A (2006) Ultrahigh-pressure metamorphic rocks from the Chinese continental scientific drilling project: II oxygen isotope and fluid inclusion distributions through vertical sections. *Contrib to Mineral Petrol* 152:443–458. <https://doi.org/10.1007/s00410-006-0084-5>
- Yoshida K, Hirajima T, Miyake A et al (2016) Combined FIB micro-sampling and X-ray microtomography: a powerful tool for the

- study of tiny fluid inclusions. *Eur J Mineral* 28:245–256. <https://doi.org/10.1127/ejm/2015/0027-2498>
- Yoshida K, Orozbaev R, Hirajima T et al (2018) Micro-excavation and direct chemical analysis of individual fluid inclusion by cryo-FIB-SEM-EDS: Application to the UHP talc-garnet-chloritoid schist from the Makbal Metamorphic Complex, Kyrgyz Tian-Shan. *Geochem J* 52:59–67. <https://doi.org/10.2343/geochemj.2.0502>
- Zhang Z, Shen K, Xiao Y et al (2005) Fluid composition and evolution attending uhp metamorphism: study of fluid inclusions from drill cores, southern sulu belt, Eastern China. *Int Geol Rev* 47:297–309. <https://doi.org/10.2747/0020-6814.47.3.297>
- Zhang Z, Shen K, Xiao Y et al (2006) Mineral and fluid inclusions in zircon of UHP metamorphic rocks from the CCSD-main drill hole: a record of metamorphism and fluid activity. *Lithos* 92:378–398. <https://doi.org/10.1016/j.lithos.2006.04.003>
- Zhang ZM, Shen K, Sun WD et al (2008) Fluids in deeply subducted continental crust: Petrology, mineral chemistry and fluid inclusion of UHP metamorphic veins from the Sulu orogen, eastern China. *Geochim Cosmochim Acta* 72:3200–3228. <https://doi.org/10.1016/j.gca.2008.04.014>
- Zhang RY, Liou JG, Omori S et al (2012) Tale of the Kulet eclogite from the Kokchetav Massive, Kazakhstan: Initial tectonic setting and transition from amphibolite to eclogite. *J Metamorph Geol* 30:537–559. <https://doi.org/10.1111/j.1525-1314.2012.00980.x>

Publisher's Note Springer Nature remains neutral with regard to jurisdictional claims in published maps and institutional affiliations.